







#### UNIVERSITATEA TEHNICA DE CONSTRUCTII BUCURESTI

Facultatea de Inginerie a Instalatiilor

Departamentul de Sisteme Termo-Hidraulice si Protectia Atmosferei

## **RESEARCH REPORT 3**

## NUMERICAL STUDY ON GLAZED SOLAR AIR COLLECTORS AND SMART INTEGRATION IN FACADE SYSTEMS

#### PhD stundent

Ing. Catalin-Ionut SIMA

Scientific coordinator

Conf. univ. dr. ing. Catalin TEODOSIU

BUCHAREST 2021

## **Table of content**

| L       | st of figures   | 3  |
|---------|---|----|
| L       | st of tables  | 4  |
| S       | ummary  | 5  |
| 1.      | Introduction  | 6  |
| 2.      | Modele de calcul CFD  | 8  |
|         | 2.1 Discretization of the computational domain  | 10 |
|         | 2.1.1 Octree method   | 11 |
|         | 2.1.2 Delaunay method   | 11 |
|         | 2.1.3 Frontal method  | 11 |
|         | 2.2 Optimization of discretization  | 12 |
|         | 2.3 Adaptation of discretization  | 12 |
|         | 2.4 Turbulence models   | 12 |
|         | 2.4.1 k- ε turbulence model   | 12 |
|         | 2.4.2 k- ω turbulence model   | 13 |
|         | 2.4.3 Reynolds Stress(RSM) turbulence model   | 13 |
| 3.      | Numerical study of glazed solar collectors in the literature  | 14 |
| 4.      | Numerical study   | 18 |
|         | 4.1 The geometry  | 18 |
|         | 4.2 The construction of mesh  | 18 |
|         | 4.3 Performing simulations in Fluent  | 19 |
|         | 4.4 Boundary conditions used in simulations   | 20 |
|         | 4.5 The construction of experimental geometry   | 25 |
|         | 4.5.1 The influence of iterations on performance of simulations   | 25 |
|         | 4.5.2 The influence of the flow on the efficiency of glazed solar collector   | 27 |
|         | 4.5.3 The influence of the distance between the glass and the absorbent plate .                                     | 28 |
|         | 4.5.4 Influence of the absorption coefficient of the perforated plate and the transmission coefficient of the glass | 30 |
|         | 4.5.5 The influence of turbulence patterns  | 32 |
| 5.<br>g | Comparative numerical study to determine the optimal configuration of the azed solar collector                      | 36 |
|         | 5.1 Simulation results  | 37 |
| 6.      | Conclusions   | 40 |
| 7.      | Conferinte si publicatii  | 41 |
| 8.      | Referinte Bibliografice:  | 42 |

## List of figures

| Figure 1 The relationship between CFD, theory and the experimental model [23]                  | 8   |
|--|-----|
| Figure 2 Structured discretization[24]   | 11  |
| Figure 3 The structure of the solar collector used in Charvart's simulations [28]              | 14  |
| Figure 4 The collector models used by Gao et al. in the simulations performed [11]             | 15  |
| Figure 5 The numerical model and the mesh of the room where the simulations were               |     |
| performed [29]   | 16  |
| Figure 6 Temperature obtained by using the solar collector as a ventilation system for 27      |     |
| Dec. [29]  |     |
| Figure 7 Temperature difference and collector efficiency depending on inlet temperature a      | and |
| air temperature [29]   | 16  |
| Figure 8 Temperature difference and collector efficiency depending on air flow and solar       |     |
| radiation intensity [29]   |     |
| Figure 9 Solar collector geometry and mesh representation                                      |     |
| Figure 10 Geometry made in DesignModeler (a), Velocity profile (b)                             |     |
| Figure 11 Temperature contour for the preliminary geometry model of 30mm and 100mm             | 22  |
| Figure 12 Velocity contour for the preliminary geometry model of 30mm and 100mm                | 22  |
| Figure 13 Final geometry and evolution of calculations in ANSYS Fluent                         | 25  |
| Figure 14 Temperature at the outlet of the solar collector depending on the number of          |     |
| iterations   |     |
| Figure 15 Velocity at the exit of the solar collector depending on the number of iterations    |     |
| Figure 16 Temperature profile according to the studied flows                                   |     |
| Figure 17 Temperature evolution depending on the air flow                                      | 28  |
| Figure 18 The evolution of the efficiency and effectiveness of the solar collector dependin    | -   |
| on the flow  |     |
| Figure 19 Temperature and velocity profile for 30mm and 50mm configurations                    |     |
| Figure 20 The influence of the distance from the temperature difference                        |     |
| Figure 21 The influence of the distance from the temperature of the perforated plate           |     |
| Figure 22 Efficiency and effectiveness of the solar collector                                  | 30  |
| Figure 23 Influence of the absorption coefficient of the perforated plate on the plate         |     |
| temperature and the outlet temperature   |     |
| Figure 24 The influence of the transmission coefficient of the glass on the plate temperature  | ıre |
| and the outlet temperature   | 31  |
| Figure 25 Turbulence models - temperature profile in the solar collector                       |     |
| Figure 26 Turbulence models - velocity profile in the solar collector                          |     |
| Figure 27 The temperature difference between the inlet and the outlet of the solar collectors. |     |
| depending on the turbulence model  |     |
| Figure 28 Average temperature of the perforated plate depending on the turbulence mode         |     |
| Figure 29 The efficiency of the solar collector depending on the turbulence model              |     |
| Figure 30 Solar collector efficiency depending on the turbulence model                         |     |
| Figure 31 Geometry of the studied solar collector  |     |
| Figure 32 Making the mesh 2,950,000 tetrahedral elements                                       |     |
| Figure 33 Heat extracted according to flow - distance study                                    |     |
| Figure 34 Efficiency of the solar collector depending on the flow - distance study             |     |
| Figure 35 Pressure loss depending on air flow - distance study                                 | 39  |

## List of tables

| Table 1 Boundary conditions  | 21           |
|--|--------------|
| Table 2 Parameters used in numerical simulations - distance study                          | 21           |
| Table 3 Simulation results in ANSYS Fluent - distance study                                | 23           |
| Table 4 Calculation of parameters - distance study   | 24           |
| Table 5 Parameters used in numerical simulations - influence of iterations                 | 25           |
| Table 6 Influence of the number of iterations on temperature and velocity                  | 26           |
| Table 7 Parameters used in numerical simulations - influence of air flow                   | 27           |
| Table 8 Parameters used in numerical simulations - influence of the distance between the   | <del>)</del> |
| glass and the absorbent plate  | 28           |
| Table 9 Parameters used in numerical simulations - influence of the absorption coefficient | t of         |
| the perforated plate and the transmission coefficient of the glass                         | 31           |
| Table 10 Temperature and velocity field for 30mm configuration                             | 37           |
| Table 11 Temperature and velocity field for 50mm configuration                             | 38           |
|  |              |

#### Summary

This paper is the third and final research report in doctoral studies and presents the numerical study conducted so far.

The paper is composed of the bibliographic analysis of the glazed solar collectors, the presentation and construction of the numerical model of the glazed solar collector, the study of data obtained from numerical simulation as well as the conclusions from the numerical study.

The building sector is a major consumer of energy worldwide, having impact on the environment through high CO<sub>2</sub> emissions, so it is important to implement solutions that help reduce greenhouse gases, high-performance solutions such as solar collectors perforated glazing that uses the energy received from the sun.

This paper highlights the opportunity to implement perforated glazed solar collectors in buildings, a system that has the potential to contribute to reducing energy consumption for space heating, reducing energy consumption for heating fresh air needed by building occupants, maintaining a guard temperature inside buildings and improving interior thermal comfort.

The present research report aims at the numerical analysis of perforated glazed solar collectors as well as the improvement of the efficiency of solar collectors by studying the different configurations of solar collectors.

After completing the numerical studies, it was found that the GTC with the configuration of 30 mm is more efficient than the GTC with the configuration of 50 mm. The efficiency of heat exchange in the case of the 30mm configuration is between 50% and 61% and for the 50mm configuration is between 41% and 54%. Regarding the overall efficiency of the collector with a smaller distance between the absorbent plate and the glass layer, it turned out to be higher with a value between 5% and 10%.

The last chapter of this numerical report captures the conclusions and perspectives of research development as well as future research directions. This numerical study will continue within the doctoral study program with the economic study and investment amortization with the future perspective of implementing perforated glazed solar collectors in buildings, part of a research project developed in the laboratories of the Faculty of Installation Engineering, Technical University of Constructions in Bucharest.

The following sources were used for the bibliographic study as well as for the study of other experimental works: www.sciencedirect.com, www.anelis.ro, www.enformation.ro, www.scholar.google.com and www.researchgate.net.

#### 1. Introduction

World energy consumption is constantly growing, it is estimated that by 2040 total energy consumption will increase by 25% compared to 2014 and by 48% compared to 2012. [1] [2]

The analyzes anticipate an average annual increase in the use of renewable energy sources of 2.6% for 2012 and 2014, thus based on the fact that renewable energy sources will have an increasingly important share in covering this global energy requirements. [2]

An analysis of climate change shows that a new record of global average temperature increases has been reached based on the values recorded for 2016. The year 2021 is the year in which a new temperature record was recorded compared to previous years, the main cause of this increases is the increase of the degree of pollution of the atmosphere of our planet. [3]

The building sector is among the main energy consuming areas representing approximately 40% of total energy consumption and 36% of total greenhouse gas emissions. Thus, the building sector enjoys a special interest in the implementation of solutions to increase energy efficiency, solutions that use renewable energy sources. [4] [5]

The sun is an important source of renewable energy, such equipment that uses radiation from the sun are solar thermal collectors. These collectors are characterized by the fluid used to use the energy from the sun, in general these collectors are divided into two main areas: solar air collectors and solar water collectors. While variants of solar water collectors have been studied in detail and optimized, used mainly in the preparation of domestic hot water, solar air collectors are very little exploited, being generally used for drying applications and for preheating the ventilation air for greenhouses and other constructions.

Solar air collectors have an advantage compared to those that use water as a fluid, in the version of collectors that use water there is the possibility of freezing, can have an impact on the environment due to fluid leakage, the investment is higher and requires maintenance. [6]

From a constructive point of view, solar thermal air collectors are classified into the following main types [7]:

- 1. opaque solar collectors
- 2. transparent solar collectors (glazed)

Glazed solar collectors may have a flat absorbent element or a thermal mass as collectors that have integrated heat-changing materials inside, but they can also be construction elements such as the Trombe wall. [8] The principle of operation of all collectors is the same, solar radiation is captured by an absorbent element that can be perforated, metallic, etc. then the heat is given to the air circulating inside the solar collector later being introduced into the building or systems. The variants of collectors with phase change materials improve the performance of the collector, these offering

a stabilization of the introduced air temperature. During the summer they can be used as buffer spaces to reduce energy consumption.

Solar collectors can reach quite high temperatures, the introduced air reaching up to 65 °C [9], studies in the literature show that these solutions can have a high potential in reducing energy consumption and can be used for various applications such as heating. / cooling, air preheating, drying, etc. [10]. The use of solar collectors with perforated absorbent plate is recommended for areas where high temperatures are used and in climates where they are not very cold, with low intensity winds. [11]

Solar collectors can be easily integrated into the construction envelope, can be integrated at the level of the exterior wall, at the level of the roof forming facades or ventilated roofs [12] - [15], these can be used to increase the efficiency of systems such as heat pumps. [16] [17]

Basically, solar thermal collectors with air represent solutions with low investment costs, the opaque variants with perforated absorbent element being characterized among the best results in terms of cost / benefit ratio in terms of reducing energy consumption for heating and ventilation. [18]

Studies in the literature show that the thermal performance of solar air collectors that use glass are much higher than simple solar collectors. Glass solar collectors help reduce energy consumption, proving to be much more efficient in cold climates than perforated solar collectors. [19] [20]

The main problem identified by Bohumi Nabilek et al [20] is that perforated solar collectors are sensitive to outdoor weather conditions, so for days with lower outdoor temperatures (between 10 °C and 23 °C) the efficiency of the GTC collector has been maintained. around 60.1%, instead the TSC type collector obtained an efficiency of only 21%.

On the other hand, it has been shown that the placement of the glass layer on the outside does not change the performance of the solar collector, but it leads to an increase in the temperature of the solar collector. [21]

Studies in the literature presented above show the importance of applying a layer of glass and canceling the effect of the wind so the layer of glass can increase the efficiency of the solar collector by over 13% and its outlet temperature by 3-4 °C. [15] [19]

In conclusion, for solving the problems induced by the cold climate of Romania and problems introduced by the high wind speeds on the perforated solar collectors, a viable and easy solution is the introduction of a layer of glass in front of the solar collector.

This solution was applied and studied in this report, a report aimed at the numerical study of the behavior of a glass solar collector.

#### 2. Modele de calcul CFD

Computational Fluid Dynamics or CFD is a branch of fluid mechanics that studies the flow of fluids and their thermodynamic properties using mathematical models. Numerical modeling of fluids is based on the flow equations that were defined by the two Navier-Stokes researchers, in addition, if the viscosity of the fluid is eliminated from these equations, then Euler's equations will result.

CFD is a computer simulation that analyzes the phenomena and predictions associated with systems involving fluid flow, heat transfer and associated phenomena (chemical reactions), thus covering a wide range of both industrial and non-industrial fields such as [22]:

- Aerodynamics, both for airplanes and cars;
- Hydro-dynamics of vessels;
- · Cooling and heating of spaces;
- Ventilation of spaces;
- Study of wind turbines;
- Distribution of pollutants in the environment;
- Weather forecast:
- Biomedicine by the flow of blood through the veins. [22]

CFD has an important role in making predictions regarding fluid dynamics, it is considered as the "third dimension" in fluid dynamics, the other two dimensions being experimental and theoretical, thus creating a relationship between the three important elements, the experimental, theoretical and numerical (CFD) being defined in the image

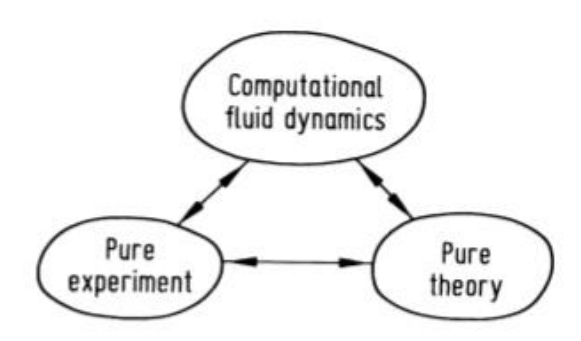


Figure 1 The relationship between CFD, theory and the experimental model [23]

By using the CFD, Chapman showed in 1979 that the investments were significantly reduced compared to a wind tunnel, with the modern computer having a much higher computing power than in 1979 and at a relatively low cost, being available to everyone. The CFD has proven to be a tool that makes the connection between pure theory and the experimental model, by validating the numerical model, calculations and predictions can be made later very easy than the experimental situation in which favorable environment must be created. [23]

One of the areas in which CFD has developed the most is the aerodynamic field in which it has proven to be much more economical to create and measure different aircraft models than to measure in a wind tunnel. [23]

The main advantages that helped and encouraged the development of CFD over the approaches based on the experimental study were:

- Reducing the realization time and costs for building new models;
- Controlling the external and internal environment for systems;
- Creating borderline situations without endangering staff, conducting studies on various accidents, safety studies, etc.;
- Control of results and their detailing. [22]

The main stages in CFD modeling and simulation that solve fluid flow problems is divided into three major stages:

- 1. "Pre-processor" is the stage that involves defining the system studied, the field of use, defining the mesh or discretization, the number of cells, their volume, geometry, selecting the type of model, physical, chemical, defining the properties of the fluid as well as the initial conditions or the boundary conditions [22]
- 2. **"Solver"** is the step that effectively involves the numerical solution of the equations introduced above. At this stage takes place the integration of the equations governing the motion of the fluid on all finite elements, the conversion of integral equations into algebraic equations and their solution by an iterative method. [22]
- 3. "**Post-processor**" represents the stage of processing and analysis of results and their transformation into graphic elements or methods of interpretation. [22]

The physical flow of any fluid is based on the three fundamental principles:

- 1. Conservation of mass
- 2. Newton's second law (F = ma)
- 3. Energy is conserved

If simplifying assumptions are applied to these three principles as a singlephase, Newtonian fluid, it is in a gravitational field, has a constant viscosity and is incompressible, these principles can be transcribed in the following equations [22]:

1. The equation of continuity or conservation mass of a fluid [22]:

$$\frac{\partial \rho}{\partial t} + \frac{\partial (\rho u)}{\partial x} + \frac{\partial (\rho v)}{\partial y} + \frac{\partial (\rho w)}{\partial z} = 0 \quad (1)$$

Written in vector form:

$$\frac{\partial \rho}{\partial t} + div(\rho \mathbf{u}) = 0 \quad (2)$$

For  $\rho$  = constant, ie incompressible fluids the equation is simplified:

$$div \mathbf{u} = 0 \quad (3)$$

Written in numerical form:

$$\frac{\partial(\rho u)}{\partial x} + \frac{\partial(\rho v)}{\partial y} + \frac{\partial(\rho w)}{\partial z} = 0 \qquad (4)$$

#### 2. The Navier-Stokes equation for conserving motion quantities [22]:

$$\rho \frac{Du}{Dt} = \frac{\partial p}{\partial x} + div(\mu \ grad \ u) + S_{Mx} \quad (5)$$

$$\rho \frac{Dv}{Dt} = \frac{\partial p}{\partial y} + div(\mu \ grad \ v) + S_{My} \quad (6)$$

$$\rho \frac{Dw}{Dt} = \frac{\partial p}{\partial z} + div(\mu \ grad \ w) + S_{Mz} \quad (7)$$

#### 3. The energy conservation equation [22]:

$$\rho c \left( \frac{\partial \mathbf{T}}{\partial t} + u_i \frac{\partial \mathbf{T}}{\partial x_i} \right) = \frac{\partial}{\partial x_i} \left( \lambda \frac{\partial \mathbf{T}}{\partial x_i} \right) + q^{\prime\prime\prime} + \mu \Phi \qquad (8)$$

#### 2.1 Discretization of the computational domain

An important step in performing a CFD simulation is the discretization of the computational domain, this procedure being based on partial differential equations, so a first step for performing a CFD simulation is to discretize the geometric model. [24]

A discretization network represents the replacement of these physical-mathematical equations with a lot of finite elements. The geometric models used in the discretization process can have different shapes, the most common shapes of the finite element are triangle and patrolled for problems using 2D models and for 3D models tetrahedral or parallelepiped shapes are used. [24]

Another classification of the type of discretization can be made depending on the type of realization of this network that can be structured or unstructured. Structured networks are generally made up of rectangles, with finite connectivity, they can also be identified as grid-type networks. Unstructured networks are generally made up of triangle or tetrahedral elements, the connectivity of this network being some. Each peak in a structured network has the same number of elements instead of an unstructured network it consists of a finite but different number. [24]

The type of element and discretization network is chosen according to the studied geometry, in general structured networks were used among the first discretization techniques, but due to the evolution of computing power and for a better understanding of the studied phenomena, generally unstructured networks are used. 24]

Over time, several methods of generating these types of networks have been used to generate unstructured discretization networks. The most well-known methods of generating three methods are identified: the octree method, the Delaunay method and the frontal method. [25]

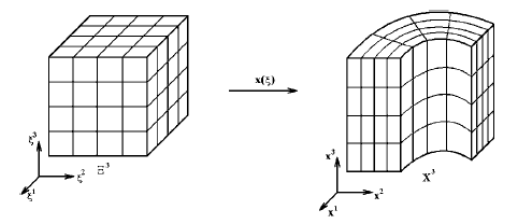


Figure 2 Structured discretization[24]

#### 2.1.1 Octree method

The octree method is a method of generating unstructured networks, it is based on a normal network of cubic cells that are divided recursively until a necessary discretization of the calculation is reached, in the end these cells are passed through a process of triangulation. This method has a very big disadvantage in terms of capturing the phenomena at the level of the boundary layer, being an old method developed 30-40 years ago. [25] [24]

#### 2.1.2 Delaunay method

It was developed by Delaunay, which is based on the connectivity of the points of a tetrahedral shape so that all four nodes of this developed tetrahedral cell fit into a closed sphere and do not contain other points. It is one of the most used methods for generating unstructured networks, being a classic method for generating discretizations. An advantage of this discretization method is the insertion of internal discretization points, a process that leads to a refinement of the discretization, a solution that can solve the problems of the boundary layer. This method of inserting new points is done with Watson and Rebay increment algorithms [24] [25]

#### 2.1.3 Frontal method

The frontal method is based on discrediting the geometry starting from an initial front, this type of discretization is done step by step by inserting new points based on the existing ones. In the case of this type of discretization, convergence problems appear, generally encountered in 3D models. It should considering for this type of discretization the configurations made must be analyzed if they are completed. In the case of these discretizations, there may be areas of "blockages" where points necessary to complete the new discretization will be inserted. [24]

All the methods presented above are methods that automatically generate the discretization of the geometry but they do not ensure a sufficient quality for performing numerical simulations. That is why the user's intervention is needed to refine the discretization model. In order to define the quality level of the discretization there are defined criteria, an example is "**cell equivolume skew**" being defined by the following formula [24]:

$$CES = \frac{V_{element-optimal} - V_{element}}{V_{element-optimal}}$$
 (9)

where:

Velement-optimal -> represents the volume of the optimal equilateral element;

V<sub>element</sub> -> the volume of the studied element.

The value of the CES coefficient equal to zero represents the optimal value, which means that a model like a CES close to zero is a model with a high quality. [24]

#### 2.2 Optimization of discretization

For the optimization of discretization networks, two optimization methods are identified:

- Optimization method with fixed connectivity, this method keeps the connectivity but will change the position of the peaks.
- Fixed position optimization method, this method keeps the position of the peaks but will change the connectivity between them. [24]

#### 2.3 Adaptation of discretization

A last procedure regarding the definition of a correct discretization model is the procedure for adapting the discretization networks, this procedure takes into account the size and density of the calculation nodes. Such methods are used for areas where we have to capture various local phenomena such as the boundary layer. [24]

For a correct adaptation of the discretization model, the nature and the phenomena that can occur within the geometry must be studied. This adaptation can be done even after completing the model and running the program of several iterations. In general, there are 3 ways to adapt discretization networks [24]:

- Subdivision of the sides of the discretization elements, the method that is achieved by dividing a side into two discretization elements;
- Direct subdivision of discretization elements, the method that is achieved by inserting a dot on each of the sides;
- The insertion of new points in the discretization network, which is effectively achieved by introducing new points and the local refining of the discretization networks. This repetitive applied procedure can affect the quality of the elements in the discretization structure. [24]

#### 2.4 Turbulence models

Among the most well-known turbulence models applied in the calculation program, the following models are identified:

- **k- ε model** (2 equations)
  - k- ε Standard
  - o k-εRNG
  - k- ε Feasible
- **k- ω model** (2 equations)
  - k- ω standard
  - o k-ωSST
- Reynolds Stress Model (7 equations)

#### 2.4.1 k- ε turbulence model

The k-  $\epsilon$  turbulence model uses two equations that solve two variables, k the kinetic energy of the turbulence and the dispersion rate of the kinetic energy  $\epsilon$  (epsilon) and starts from the premise that the turbulence regime is stable an entire domain and the viscosity it is negligible, based on Boussinesq's hypothesis. [26]

This model does not calculate very precisely the flow fields that have unfavorable pressure gradients behaving well with complex geometries for eternal flow problems, further it is divided into 3 types of models:

- The k-ε Standard model is an easy-to-use model that does not consume much memory for simulations, it is not accurate but approximate results can be obtained for a first preliminary study. [26]
- The k- ε RNG model takes into account smaller turbulence scales in the calculation model, thus providing better results for areas where turbulence occurs near the wall. [26]
- The **k-ε Realizable** model is a model introduced by Lumley, so the concept of "realizable" refers to the fact that the model respects certain mathematical constraints in the physical model of turbulence. Thus, this model can more accurately predict the rate of spread of both flat and vortex (round) jets. Also, this turbulence model offers superior performance to simulations involving boundary layers, turbulence, pressure gradients, etc. [26]

#### 2.4.2 k- ω turbulence model

The second tubulence model corresponds to the k-  $\omega$  model being a model similar to the k-  $\epsilon$  turbulence model, but it solves the variable  $\omega$  (omega) - representing the rate of dispersion of kinetic energy. This is a model with a small number of Reynolds being used in conjunction with wall functions. It is much more nonlinear than the k-  $\epsilon$  model, being more sensitive for calculating / predicting the initial value. This model is used to the detriment of the k-  $\epsilon$  model which is not accurate for the calculation of indoor air flows, air flows which have a separate curvature or in the form of jets, such as the flow through the interior of a pipe having a curved shape. [27]

This model being characterized in turn by two other models below:

- The k-ω Standard model is based on Wilcox's model incorporating models with a low Reynolds, today solving the problems of separating the boundary layers of the standard k-ε model [26]
- The k- ω SST (Shear-Stress Transport) model was developed by Menter to effectively capture the accuracy of the k- ω model at the wall boundary with the independent free flow of the k- ε model in the far field. These features make the k-ω SST model more accurate and reliable for a wider range of flows, being considered a complete model for all flows. [26]

#### 2.4.3 Reynolds Stress(RSM) turbulence model

The last turbulence model is represented by the **Reynolds Stress Model or RSM** being the most elaborate turbulence model, which solves five transport equations in 2D models and seven transport equations in 3D models. Because it captures more phenomena by solving more equations than previous models with two equations, having a greater potential to provide predictions of complex flows. In some situations it may be that the RSM model may not always produce results that are clearly superior to the simpler models in these classes, thus adding additional costs to perform the calculations. [26]

## 3. Numerical study of glazed solar collectors in the literature

An important stage in the optimization of solar collectors is the bibliographic study and the current stage of research in the literature. Most of the studies performed on solar collectors are experimental studies and refer to the studies of perforated solar collectors (TSC), collectors that are used in climates with warm winters.

The numerical study proposed by us refers to perforated solar collectors in which a sheet of glass was attached to cancel the effects of wind on heat loss, as well as to optimize and increase the indoor temperature.

Numerical studies in the literature are quite low in terms of glazed solar collectors, these studies being conducted recently, many of these studies also refer to the integration of phase-changing materials. The integration of phase change materials in buildings is studied in detail in Andrei Bejan's thesis and is not the subject of this report.

A first study conducted by P. Charvart et al [28] was performed in the TRNSYS calculation program, it made a comparison between two glazed solar collectors, one simple and one having integrated inside the absorbent plate PCMs.

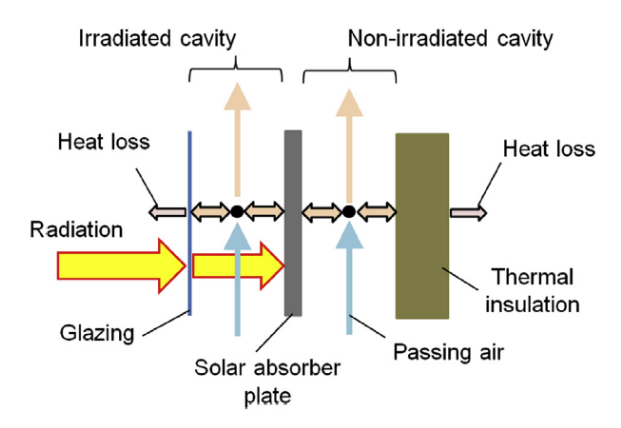


Figure 3 The structure of the solar collector used in Charvart's simulations [28]

A first conclusion of this study was that for the solar collector with integrated PCMs the efficiency is lower than for the simple glazed solar collector. One of the problems of solar collectors with integrated PCMs is that under certain conditions the intake temperature fails to reach the melting temperature of solar collectors, which remains in a solid state. PCMs with a melting point of 41 °C and an inlet temperature of 20 °C were chosen for this investigation. [28]

The results of studies conducted by Charvart et al indicate that the use of PCMs reduces fluctuations due to solar radiation, but it reduces the efficiency of the solar collector compared to a simple glazed collector. However, PCM glazed solar collectors can be used in systems where it is necessary to provide a constant temperature such as drying systems for various products. [28]

A numerical analysis by Gao et al. [11] in which it presents the simulation of three types of solar collectors with the help of the Matlab calculation program, it predicts the thermal performance of these 3 types illustrated in the figure below.

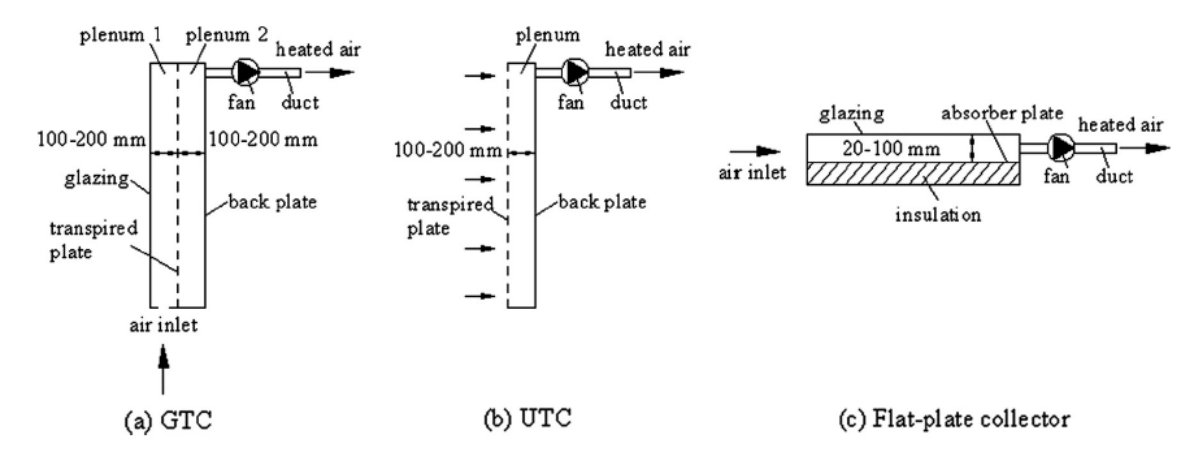


Figure 4 The collector models used by Gao et al. in the simulations performed [11]

Using a sheet of glass can reduce heat loss due to convection from high wind speeds. Thus for a radiation of 400 W/m² and a temperature of -10°C and a wind between 3 - 3.5 m/s: the temperature at the exit of the GTC is higher than that of UTC and the thermal efficiency increases from 0.36 to 0.56% depending on the pitch of the perforations. [11]

Thus for glazed solar collectors, radiation and air flow have a high impact, so the air flow must be carefully selected to meet the heating requirements of the indoor space. [11]

By using the glazed surface, an improvement of the inlet temperature is shown, more precisely an increase of 9 °C and 70%, respectively, compared to simple solar collectors, for a radiation of 400 W/m² and an external temperature of -10°C. [11]

Gao et al observed that for a reference building the use of glazed solar collectors (type a) reduced energy consumption by 20%, being twice as high for flat glazed solar collectors (type c), and nine times higher than a simple solar collector (type b), therefore a significant reduction will be obtained by using GTC type solar collectors in cold climates. [11]

Zhang et al conducted a numerical study using the Fluent simulation program, which performed a simulation of a glazed solar collector system for a room (bedroom) measuring 5.45m x 4.18m x 3.0m, with an area glazed as in the image below (figure 5). [29]

The study aimed to monitor indoor air quality and indoor pollutants, namely monitoring the concentration of  $CO_2$  from humans and the concentration of  $CO_2$  and CO from the traditional heating system "kang" (the equivalent of a stove with food preparation in Romania). For the CFD study were used k- $\epsilon$  realizable turbulence model, the radiation transfer evaluation model was DO (Discrete Ordinates), using a mesh of 881,500 elements. [29]

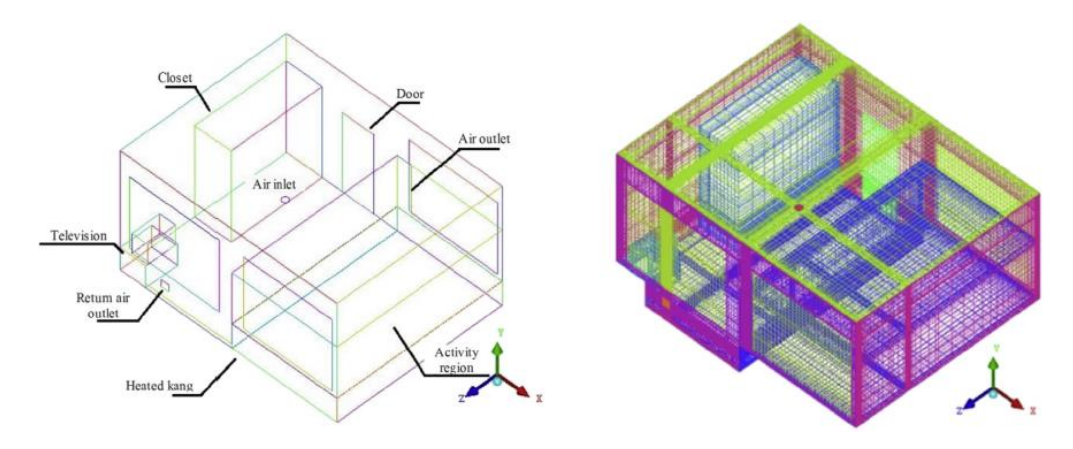


Figure 5 The numerical model and the mesh of the room where the simulations were performed [29]

For the use of the solar collector, it was observed that for outdoor temperatures between -15.8°C and -7.92°C, an increase from 15.81°C to 26.42°C is obtained, having an impact on the indoor temperature, which is between 15.40°C and 18.20°C, this study being conducted between 9:00 and 15:00 on December 27. [29]

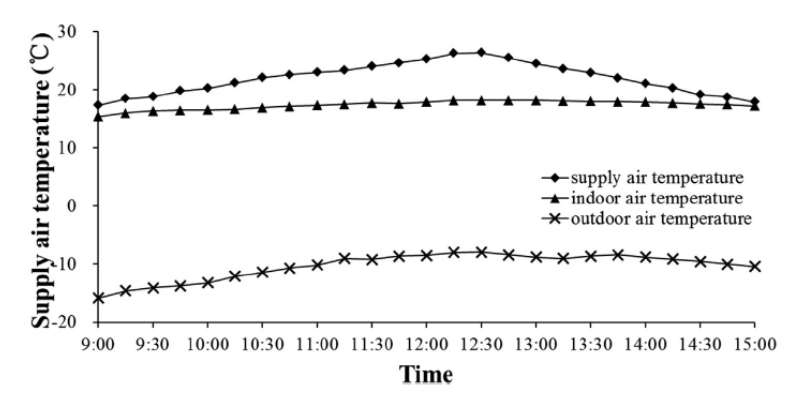


Figure 6 Temperature obtained by using the solar collector as a ventilation system for 27 Dec. [29]

As a general conclusion on the study, GTC brings significant reductions in energy consumption, but more importantly it increases indoor air quality for houses located in rural areas and using the traditional stove system ("kang"). The GTC system being a suitable and usable solution in parallel with other systems with a very low investment. [29]

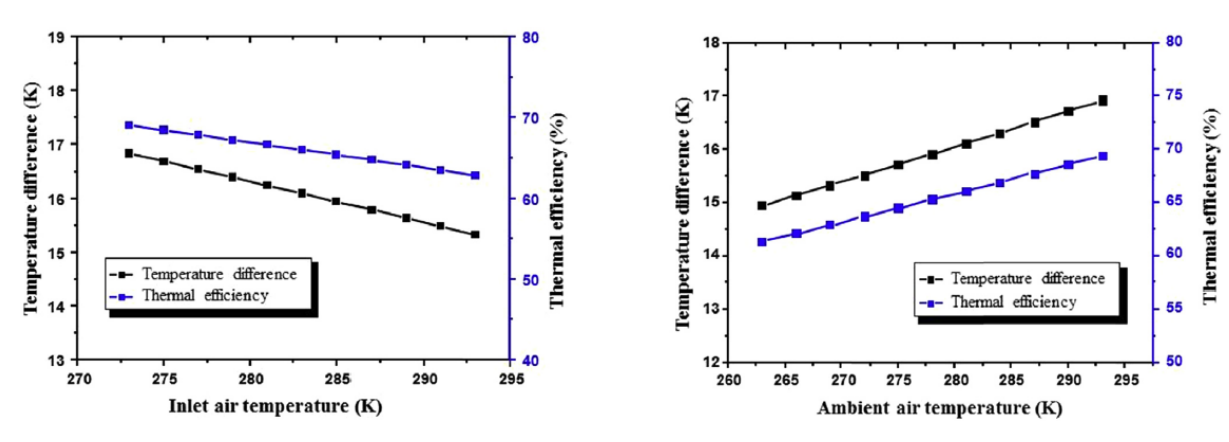
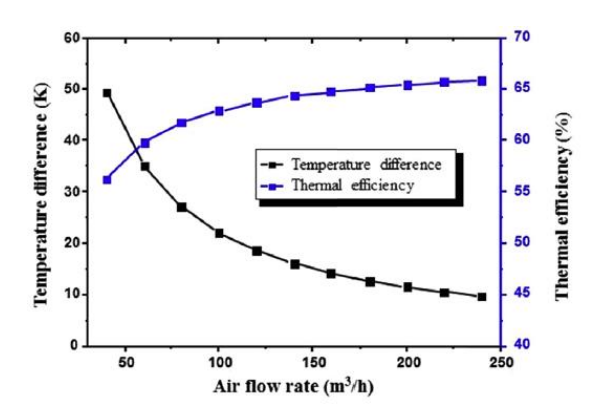


Figure 7 Temperature difference and collector efficiency depending on inlet temperature and air temperature [29]



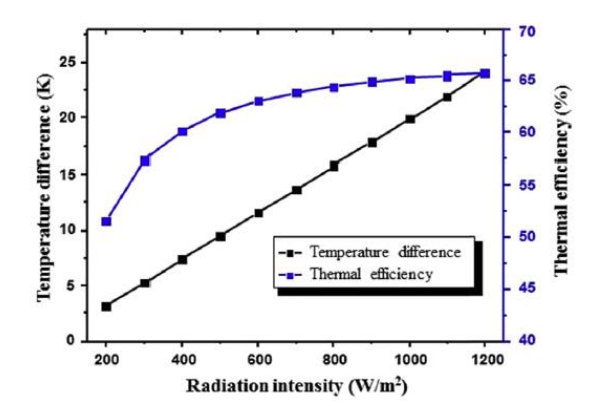


Figure 8 Temperature difference and collector efficiency depending on air flow and solar radiation intensity [29]

A numerical study carried out with the help of the Matlab calculation program, shows the influence of the temperature at the exit from the solar collector and of their efficiency depending on certain conditions. The thermal efficiency of the GTC decreases as the inlet temperature increases, this being due to the loss of heat and the decrease of the temperature difference between the absorbent plate and the outside air temperature. [19]

The increase of the air flow influences the temperature difference between the inlet temperature in the collector and the outlet temperature in the collector, an important increase of the efficiency happens for the flows between 40 m³/h and 50 m³/h thus for the flows of 200 m³/h up to at 240 m³/h the increase is insignificant of only 0.43%, this can be seen in figure 8. [19]

The thermal efficiency of the solar collector increases as radiation and temperature increase, but this improvement is not as rapid as in the case of low temperatures and radiation. [19]

### 4. Numerical study

The ANSYS - FLUENT simulation software was used to create the numerical model of the solar collector, through which different models of the solar collector were compared. The Fluent calculation software developed by ANSYS can perform numerical simulations of fluid mechanics and can obtain results close to reality at a low cost.

Until the numerical simulations are performed within the ANSYS - Fluent calculation program, it is necessary to go through several steps that will be presented below:

- 1. Realization of the studied stand geometry;
- 2. Making the mesh;
- 3. Defining the calculation equations and the boundary conditions;
- 4. Performing the actual simulation.

ANSYS is an interface that facilitates all these steps through its integrated programs and more precisely: ANSYS Workbench, ANSYS Meshing and ANSYS Fluent

#### 4.1 The geometry

The first step for studying the numerical model of the glazed solar collector is to define the correct geometry of the studied experimental model. The geometry is made with the help of the Design Modeler software or with the SpaceClaim software, available in the ANSYS Workbench.

A second possibility to define the geometry is the SolidWorks software within the CAD platform, which is then imported into the ANSYS software, the variant that was chosen in this case as well.

The geometry was made within the SolidWorks program and then imported into the DesignModeler software where the components were defined and assembled. An important detail that must be taken care of is to be careful that all the components within the geometry are interconnected in order to avoid the phenomenon of emptiness within the geometric model, which will later lead to the impossibility of running the simulation.

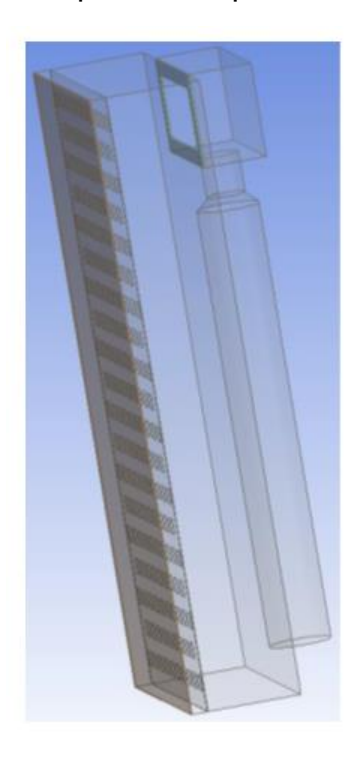
This problem was also encountered in defining the components of the solar collector, given that the solar collector model uses a perforated plate, and the solution to solve the problem was using some small elements that correspond to the air to fill the perforations in the geometric model.

#### 4.2 The construction of mesh

The next step after completing the geometry is to create the mesh in the ANSYS Meshing program, which introduces the parameters necessary for the mesh such as the program used in the simulations and the type of finite, linear, square or tetrahedral element. For the solar collector model, the tetrahedral type element was chosen because it better illustrates the phenomena near the holes in the perforated plate. The mesh used was of the CFD (Computational Fluid Dynamics) type necessary for the

simulation within the ANSYS Fluent program, the size of the elements being reduced by 20 mm. In order to obtain a mesh that would better illustrate the phenomena that occur at the level of the perforated plate and to obtain a more accurate simulation of the heat transfer between the air and the plate at the level of the perforations, the "inflation" function was used. By using this function, the number of elements in the vicinity of the plate will increase in order to better capture the region of the boundary layer for a turbulent air flow.

An important aspect in the construction of the mesh is to define the surfaces of the studied model in order to subsequently impose the boundary conditions within the Fluent software. In the case of the glazed solar collector, boundary conditions have been imposed for the inlet and outlet of air from the collector, for the glass, the perforated plate or for the walls of the solar collector. Figure 9 illustrates the geometry made in SolidWorks and the mesh made in ANSYS Meshing, for the model with the distance between the perforated plate and the 50 mm glass.



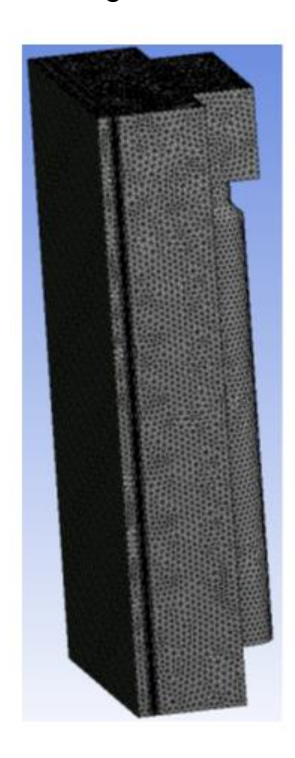
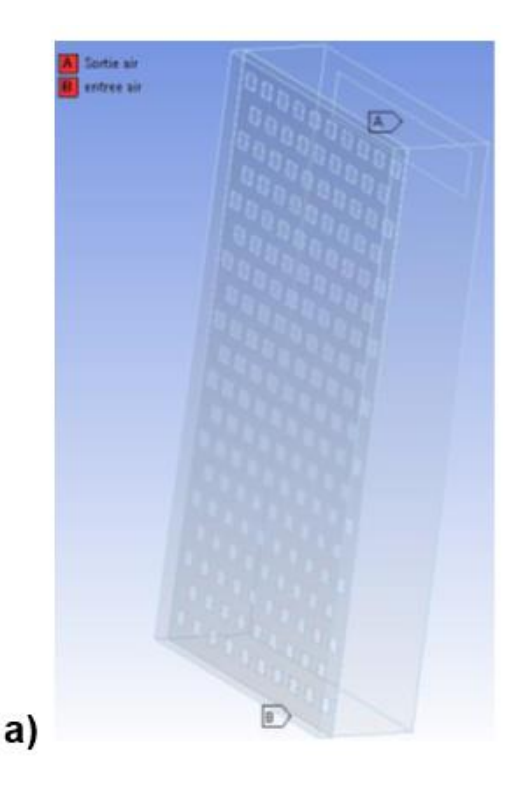


Figure 9 Solar collector geometry and mesh representation

#### 4.3 Performing simulations in Fluent

The last software used for the simulations is Ansys Fluent, in this software the definition of the equations used in the simulations and the limit conditions used takes place. After introducing the equations and boundary conditions, the last step in defining the simulation and defining the iterations. The number of iterations during the simulation can have a great influence on the final results, so it is important that the recorded values converge and that the number of iterations is sufficient.

After completion of iterations and obtaining results whose values converge, the simulation program offers the possibility to visualize the results in graphical form, in our case a section was made inside the solar collector in which the velocity profile is illustrated.



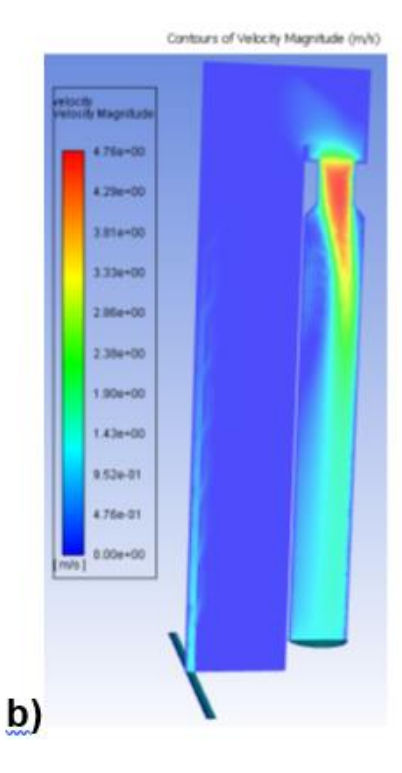


Figure 10 Geometry made in DesignModeler (a), Velocity profile (b)

This method of visualization can help to qualitatively compare the simulations performed by capturing the phenomena inside the studied solar collector. A second method of comparison is the quantitative method by comparing the average values of temperature, velocity or heat transfer of an element in the solar collector such as the perforated plate or the exit from the solar collector.

By obtaining average values we can see if the simulation was performed correctly by interpreting them and if they fall within our range of interest. The values recorded during the simulations were the following:

- Average perforated plate temperature (° C)
- Average temperature at the exit of the solar collector (° C)
- Heat exchange coefficient of the perforated plate h (W / m2. K)
- Heat transfer at the level of the perforated plate. φ (W / m2)

An important parameter in the validation of the results is the y + value of the perforated plate, this is a dimensionless value that characterizes the behavior of the fluid velocity near a wall. A high value of the y + coefficient could mean that the software has problems with the interaction of the fluid with a wall, which will require a mesh with a finer discretization or a different turbulence pattern.

#### 4.4 Boundary conditions used in simulations

A first numerical model of the solar collector was made with a simplified geometry, thus having the collector output not modeled as figure 10. These comparative simulations were made to familiarize with the calculation program and to compare numerical models, the collector output being only a the air transfer area, the femomen which is interesting for the solar collector takes place at the level of the glass and the perforated plate. The boundary conditions are illustrated below:

Table 1 Boundary conditions

| -          | Parameters | Values                    | Commentary                                  |  |
|------------|------------|---------------------------|---|--|
| Mesh       | Number     | Between 1.3 million and   | Made with Ansys Meshing with increasing     |  |
|            |            | 1.5 million items         | numbers near the "inflation" board          |  |
| General    | Regime     | Stationary                |   |  |
|            | Gravity    | - 9,81 m/s2               |   |  |
|            | Energy     | Active                    |   |  |
|            | Flow Model | RNG k-ε turbulence        |   |  |
|            |            | model with Enhanced       |   |  |
| The        |            | Wall Functions            |   |  |
| physical   | Radiation  | Surface to Surface (S2S)  | Using coordinates for Bucharest with direct |  |
| model      | Model      | model; radiation from     | solar radiation of 605.7 W / m2 and diffuse |  |
|            |            | Solar Ray                 | solar radiation of 150 W / m2               |  |
|            | Air        | Gaz ideal                 |   |  |
|            |            | ρ= 8030 kg/m <sup>3</sup> |   |  |
|            | Glass      | Cp = 502,48 J/kg K        | Transmission coefficient = 0.8              |  |
| Materials  |            | λ = 16,26 W/m K           |   |  |
|            | Perforated | ρ= 8030 kg/m <sup>3</sup> |   |  |
|            | plate      | Cp = 502,48 J/kg K        | Absorption coefficient = 0.8                |  |
|            |            | λ = 16,26 W/m K           |   |  |
|            | Collector  | Heat transfer is zero     | Heat transfer is zero due to external       |  |
| Boundary   | envelope   |                           | insulation, adiabatic process               |  |
| conditions | Inlet      | Negative velocity         |   |  |
|            |            | imposed at the entrance   |   |  |
|            |            | to the solar collector    |   |  |

The main element studied in the preliminary model was to obtain a quantitative estimate for the three studied solutions 30 mm, 50 mm and 100 mm distance between the perforated plate and the glass. The table below illustrates the parameters introduced for the values of temperature, air flow, solar radiation and studied distances.

Table 2 Parameters used in numerical simulations - distance study

|                     | Parameters             | Values           |
|---------------------|------------------------|------------------|
|                     | Air flow (m³/h)        | 200              |
| Boundary            | Inlet temperature (°C) | 25               |
| conditions          | Date                   | 21 june 13 :00   |
|                     | Solar radiation        | solar rad. 1000W |
| Variable parameters | Distance (mm)          | 30, 50 and 100   |

The simulation was performed for 1500 iterations, being possible to view the velocity and temperature profile for the 3 cases above, the comparison of the model with distance of 50 mm and distance of 100 mm was illustrated below for velocity and temperature profiles:

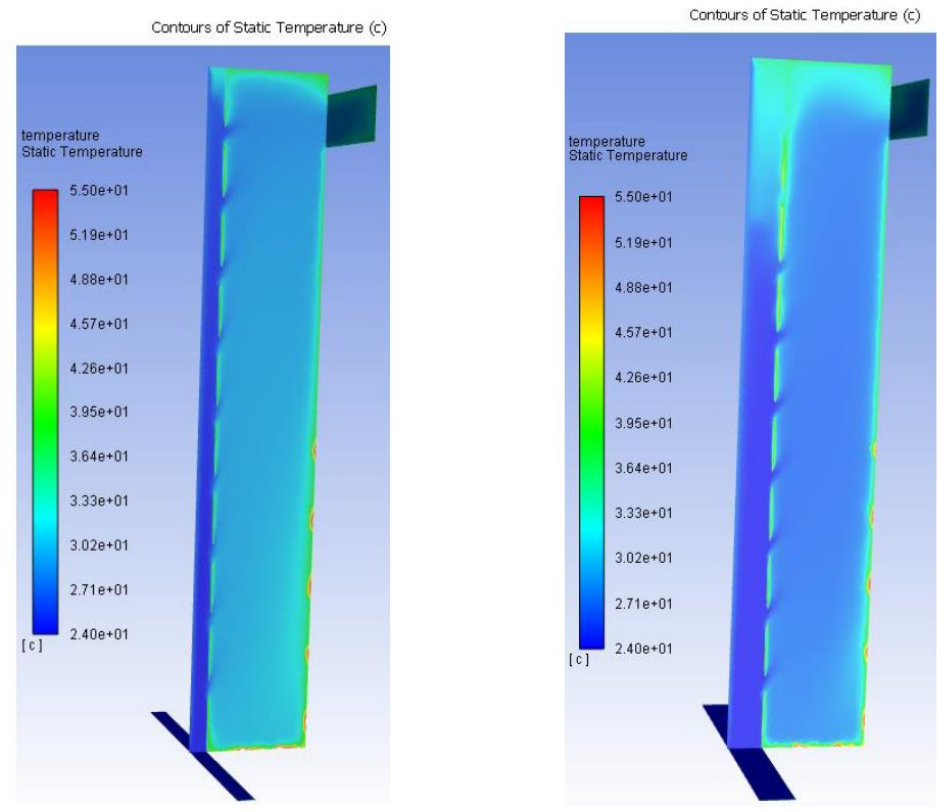


Figure 11 Temperature contour for the preliminary geometry model of 30mm and 100mm

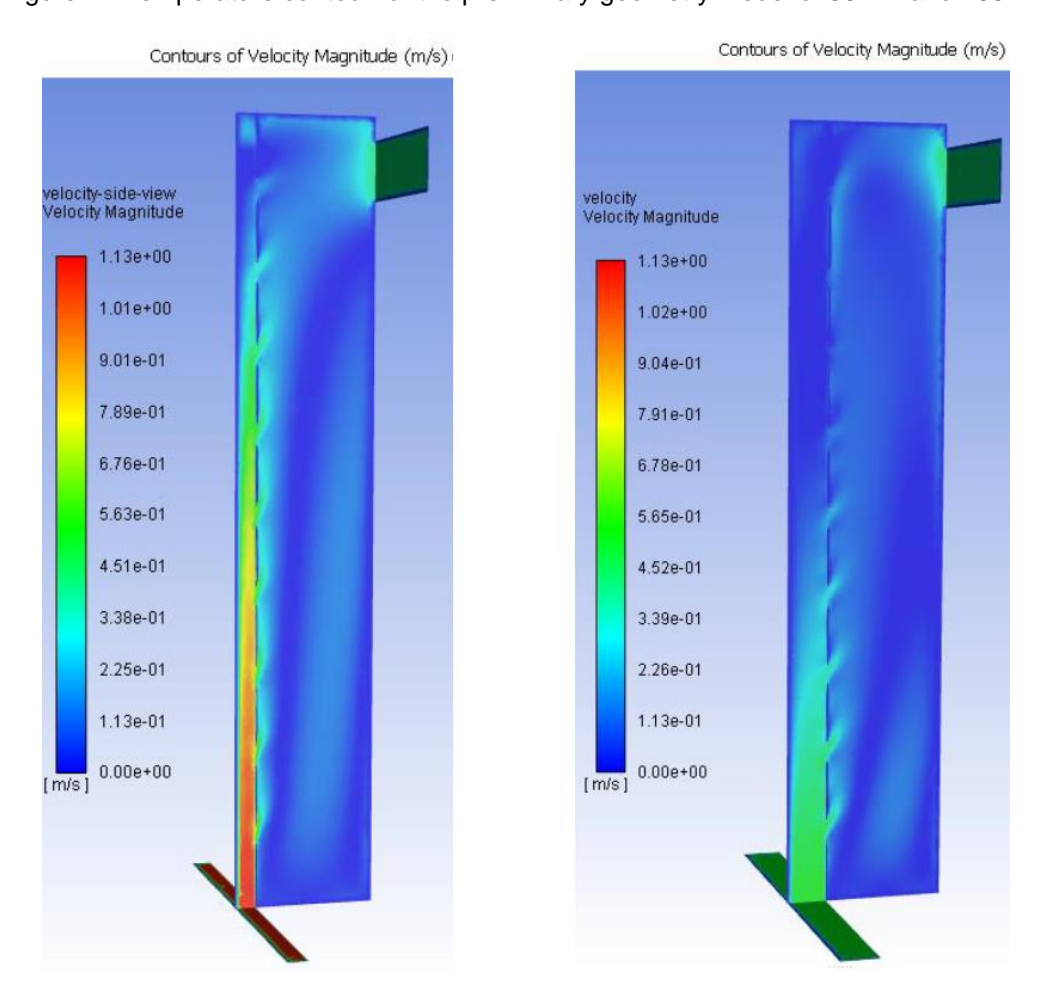


Figure 12 Velocity contour for the preliminary geometry model of 30mm and 100mm

As can be seen in the above images for the thickness of 100 mm the air velocity is lower as usual, a conclusion that can be drawn from the above images is to improve the heat flow for smaller distances between the glass and perforated plate.

Thus, in order to strengthen these conclusions for each of the models (30 mm, 50 mm and 100 mm), several parameters illustrated in the table below were calculated.

| Distance(mm)  | 100   | 50    | 30    |
|---|-------|-------|-------|
| Temperature difference (°C)                           | 5,98  | 6.78  | 7,24  |
| Plate temperature (°C)                                | 40,76 | 39,56 | 38,13 |
| Coefficient of transfer to the plate surface (W/m² K) | 4,37  | 5,16  | 5,70  |
| Heat flow (W/m²)                                      | 114,4 | 126,1 | 130,6 |
| V±  | 0.7   | 1.03  | 1 43  |

Table 3 Simulation results in ANSYS Fluent - distance study

The smaller the distance between the glass and the absorbent plate, the higher the transfer coefficient values and thus a larger temperature difference at the outlet of the collector. The temperature of the absorbent plate decreases as the distance between the plate and the glass decreases, this being due to the turbulence and the more intense exchange at the level of the absorbent plate.

In order to be able to compare the numerical models of solar collectors, the main parameters that define their performance were compared, these parameters being defined by Wang et al. [18]:

- heat exchange efficiency (εHX),
- efficiency of the solar collector (n)

$$\eta = \frac{c_{p,aer} m_{aer} (T_{aer,ev} - T_{amb})}{I_T A_S}$$
 (10)

$$\varepsilon_{HX} = \frac{T_{aer} - T_{amb}}{T_P - T_{amb}} \tag{11}$$

unde:

cpaer -> is the specific heat of the air (J/kgK),

maer -> is the mass flow of air through the manifold (kg/s),

T<sub>aer,ev</sub> -> is the temperature of the exhaust air (K),

 $T_{amb}$  -> is the ambient air temperature (K),

 $I_T$  -> is the solar radiation incident on the collector (W/m<sup>2</sup>),

As -> is the surface of the collector (m2)

T<sub>P</sub> -> is the average temperature of the absorbent plates (K).

Another calculation formula for solar collector efficiency is proposed by Van Decker et al. [30] this using the efficiency of heat exchange:

$$\eta = \frac{\alpha_s}{1 + \frac{h_r}{\varepsilon_{HX} \rho_{aer} c_{p,aer} v_s}}$$
 (12)

,where:

 $\alpha_s$  -> represents the absorption coefficient of the plate,

 $h_r$  -> is the radiative heat transfer coefficient between the plate and the environment (W/m<sup>2</sup>K),

 $\rho_{aer}$  -> is the density of the air (kg/m3),

v<sub>s</sub> -> is the surface suction velocity of the air (m/s)

Thus the term  $h_r$  in Van Decker's formula comes from Stefan-Boltzmann's formula for heat transfer exchanged between a surface and the environment.

$$\phi = \varepsilon \times \sigma \times S \times (T_S^4 - T_a^4) \tag{13}$$

,where:

ε -> the emissivity of the material

 $\sigma$  -> is the Stefan-Boltzmann constant (W/m<sup>2</sup> K<sup>4</sup>),

**S**-> is the surface of the perforated plate (m<sup>2</sup>),

 $T_s$  -> is the temperature of the plate or surface (K)

T<sub>a</sub> -> is the air temperature (K)

Because the expression implies a nonlinear form (temperatures at the fourth power), if the temperature difference is very small, the linearization of the expression can be achieved as follows [30]:

$$\phi = \varepsilon \times \sigma \times S \times (T_s - T_a)$$
 (14) cu  $h_r = 4 \times \varepsilon \times \sigma \times T_m^3$  (15)

,unde:

 $T_m$  -> is the average temperature between the air temperature Ta and the plate temperature Ts (K)

Thus the formula expressed by Van Decker for calculating the efficiency of the cholecotrous is based on the fact that the temperature difference between the absorbent plate is close to the air temperature, which implies large errors to increase the difference. The following are the parameters described above for the preliminary model [30]:

Table 4 Calculation of parameters - distance study

| Distance(mm)                                 | 100  | 50   | 30   |
|--|------|------|------|
| Heat exchange efficiency εHX (%)             | 37,9 | 46,5 | 55,1 |
| Solar collector efficiency η<br>(Wang) (%)   | 19,4 | 22,0 | 23,5 |
| Solar collector randament η (Van Decker) (%) | 77,5 | 77,9 | 78,3 |

In the glazed solar collector with a distance of 30mm the temperature difference between inlet and outlet is larger, so it can be concluded that for the preliminary model the thickness of 30mm offers the best efficiency and heat exchange between the plate and the outside air.

#### 4.5 The construction of experimental geometry

To validate the numerical model, a geometric model was made according to the real dimensions of the glazed solar collector stand. The objective of this study is to study the influence of certain parameters on the solar collector such as:

- number of iterations;
- · solar radiation;
- air flow;
- distance between the glass and the perforated plate

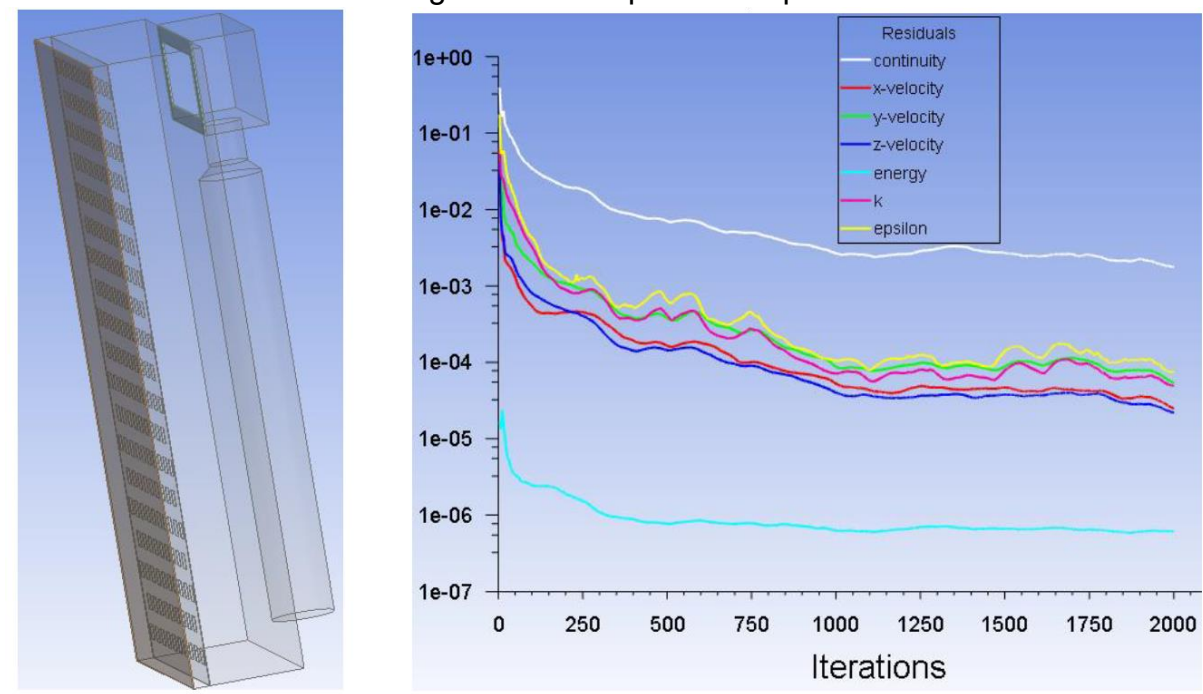


Figure 13 Final geometry and evolution of calculations in ANSYS Fluent

By adding a plenum and extending the pipe to stabilize the velocity in the pipe, it will allow a better illustration of the parameters at the output of the glazed solar collector, thus leading to more accurate results for the measured temperatures.

#### 4.5.1 The influence of iterations on performance of simulations

This study is essential for the most accurate presentation of the results from the Fluent program. The Fluent software solver starts from the initial solution and through a system that matrix algorithms obtained by discretization iterates this solution, a correct simulation is considered when the residues are very small and the results converge figure 13.

The solution is considered to be convergent if the residues stabilize during the iterations, below were illustrated the parameters used in the simulations performed.

|            | Parameters                   | Values           |
|------------|------------------------------|------------------|
|            | Air flow (m <sup>3</sup> /h) | 203              |
|            | Inlet temperature (°C)       | 26,8             |
| Boundary   | Distance(mm)                 | 30               |
| conditions | Date                         | 12 oct. 13:00    |
|            | Solar radiation              | solar rad. 785W  |
| Variable   | Number of iterations         | from 200 to 2000 |

Table 5 Parameters used in numerical simulations - influence of iterations

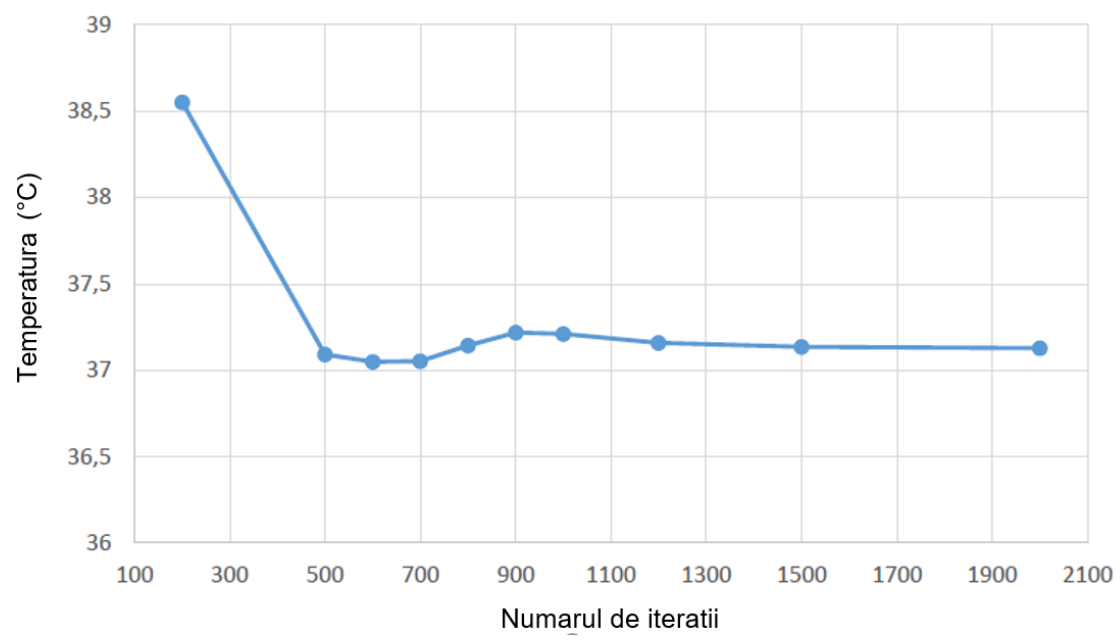


Figure 14 Temperature at the outlet of the solar collector depending on the number of iterations

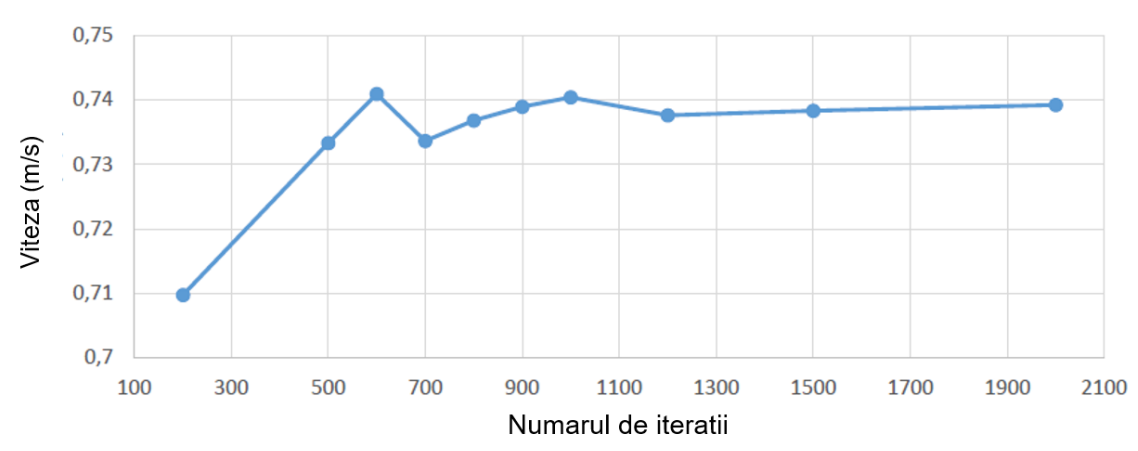


Figure 15 Velocity at the exit of the solar collector depending on the number of iterations

According to the graphs attached above, the stabilization of velocity and temperature is achieved after 1000 iterations, so the error being only 0.02% for temperature and 0.21% for velocity. For future simulations we will consider that for over 1500 iterations it is enough to obtain real results, the values for the above graphs being attached in the following table.

| Table 6 Influence of the number of iterations on t | temperature and | velocity |
|--|-----------------|----------|
|--|-----------------|----------|

| Number of iterations | Temperature (°C) | Error (%) | Velocity(m/s) | Error (%) |
|----------------------|------------------|-----------|---------------|-----------|
| 200                  | 38,552           | -         | 0,710         |           |
| 500                  | 37,091           | 3,79      | 0,733         | -3,325    |
| 600                  | 37,049           | 0,109     | 0,741         | -1,071    |
| 700                  | 37,052           | -0,008    | 0,734         | 1,029     |
| 800                  | 37,144           | -0,239    | 0,737         | -0,451    |
| 900                  | 37,218           | -0,192    | 0,739         | -0,296    |
| 1000                 | 37,210           | 0,021     | 0,740         | -0,211    |
| 1200                 | 37,158           | 0,135     | 0,738         | 0,395     |
| 1500                 | 37,135           | 0,060     | 0,738         | -0,099    |
| 2000                 | 37,127           | 0,021     | 0,739         | -0,127    |

#### 4.5.2 The influence of the flow on the efficiency of glazed solar collector

Air flow is an important parameter that can influence the heat exchange. These simulations were made for the 30 mm configuration to see the influence of the flow on this configuration, being the optimal configuration for heat transfer between the plate and the air coming from outside. The parameters introduced in the air flow study are illustrated below.

|            | Parameters                   | Values             |
|------------|------------------------------|--------------------|
|            | Inlet temperature (°C)       | 25                 |
| Boundary   | Distance(mm)                 | 30                 |
| conditions | Date                         | 11 oct. 13:00      |
|            | Solar radiation              | solar rad. 1000W   |
| Variable   | Air flow (m <sup>3</sup> /h) | 158; 203; 296; 354 |

Table 7 Parameters used in numerical simulations - influence of air flow

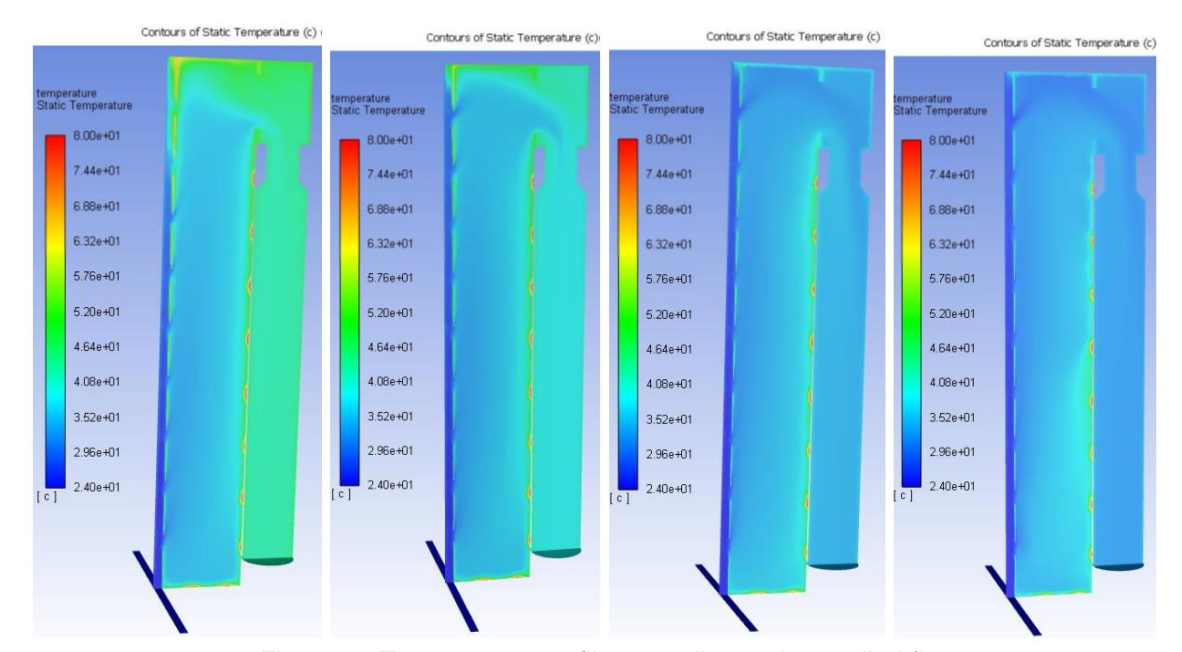


Figure 16 Temperature profile according to the studied flows

As can be seen in the images above, as the flow rate at the outlet decreases, the heat exchange at the absorbent plate increases. By increasing the air flow the air temperature decreases the efficiency of the collector decreases, however the overall efficiency of the collector increases as it extracts more heat.

Therefore, a balance must be found between the overall efficiency of the collector and the efficiency of heat exchange, as can be seen the air flow of 250 m<sup>3</sup>/h - 300 m<sup>3</sup>/h is the optimal flow for this glazed solar collector configuration. In addition, it must be taken into account that for a higher air flow the fan used will consume more energy, which is reflected in a lower efficiency of the glazed solar collector.

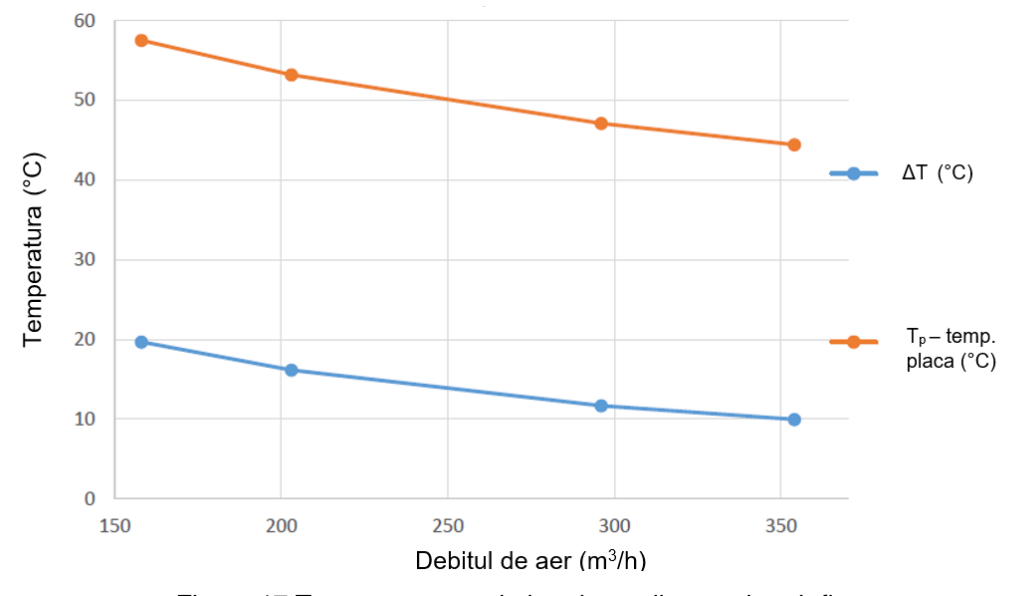


Figure 17 Temperature evolution depending on the air flow

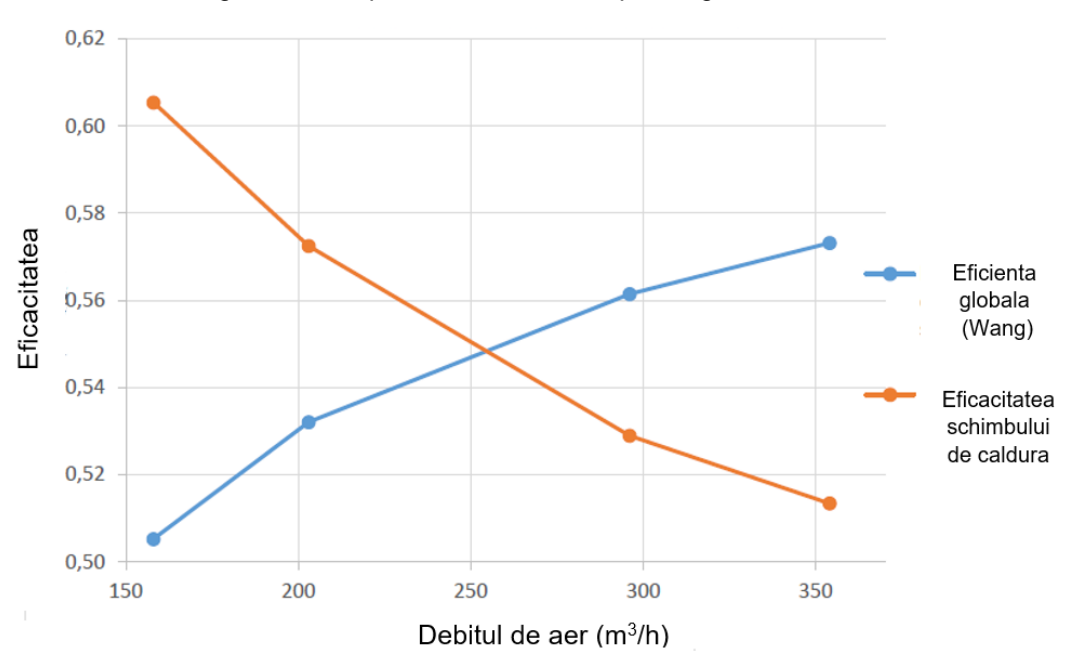


Figure 18 The evolution of the efficiency and effectiveness of the solar collector depending on the flow

#### 4.5.3 The influence of the distance between the glass and the absorbent plate

In the following, a simulation was performed to observe the influence of the distance between the glass and the perforated absorbent plate, the parameters used in the simulation were presented in the table below:

Table 8 Parameters used in numerical simulations - influence of the distance between the glass and the absorbent plate

|            | Parameters                   | Values           |
|------------|------------------------------|------------------|
|            | Inlet temperature (°C)       | 25               |
| Boundary   | Air flow (m <sup>3</sup> /h) | 158              |
| conditions | Date                         | 11 oct. 13:00    |
|            | Solar radiation              | solar rad. 1000W |
| Variable   | Distance (mm)                | 30 ; 50 ; 70     |

The same observation was made as in the case of the preliminary model, the temperature is higher in the case of the shorter distance, the velocity is different only in the area of the "air gap" between the plate and the glass.

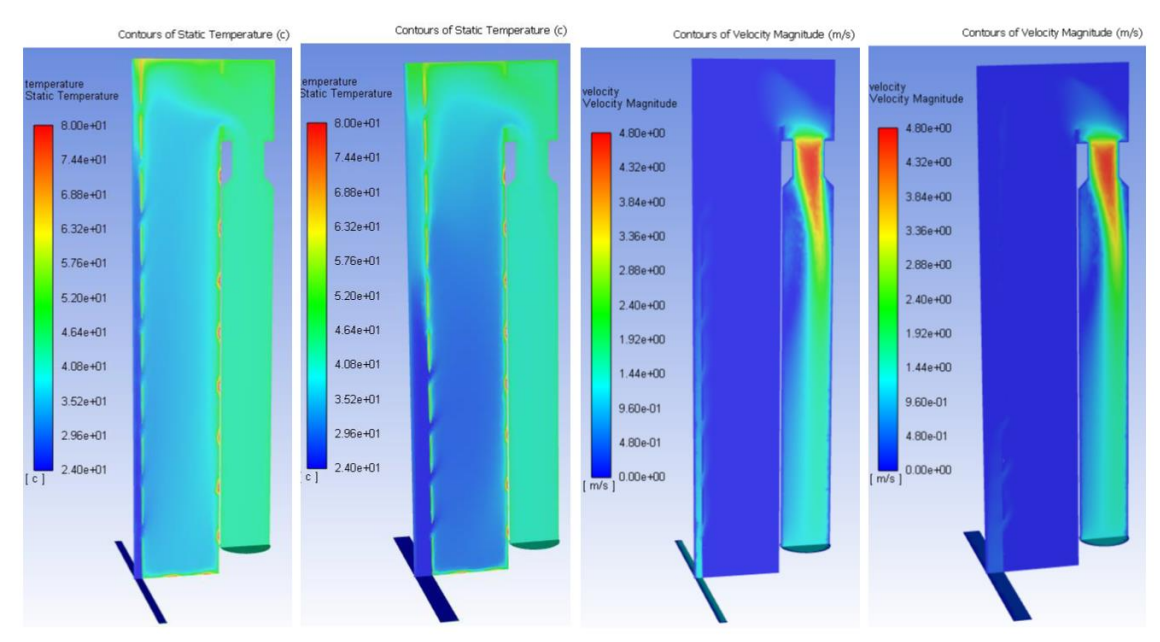


Figure 19 Temperature and velocity profile for 30mm and 50mm configurations

For a better analysis of the differences between the studied configurations, the graphs will be drawn for the study of the temperature difference between the inlet and the outlet, the absorbent plate temperature, the global efficiency and the efficiency of the heat exchange, as follows.

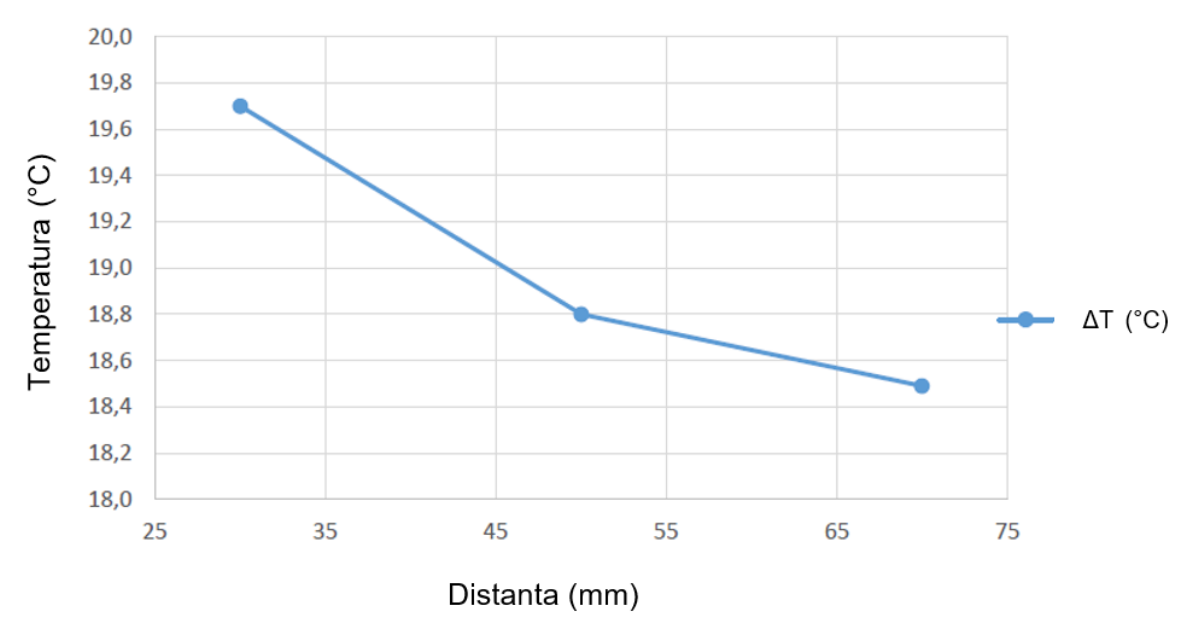


Figure 20 The influence of the distance from the temperature difference

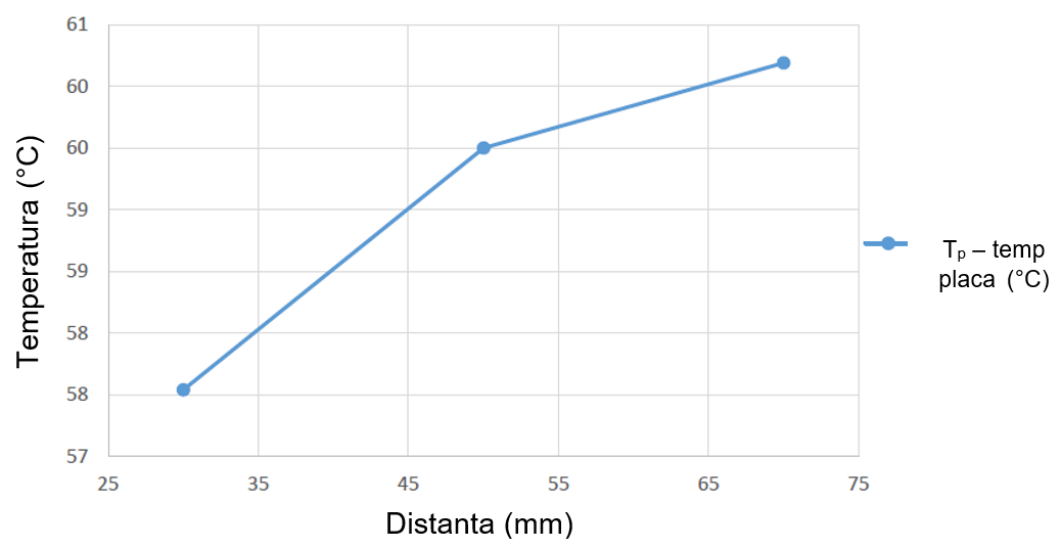


Figure 21 The influence of the distance from the temperature of the perforated plate

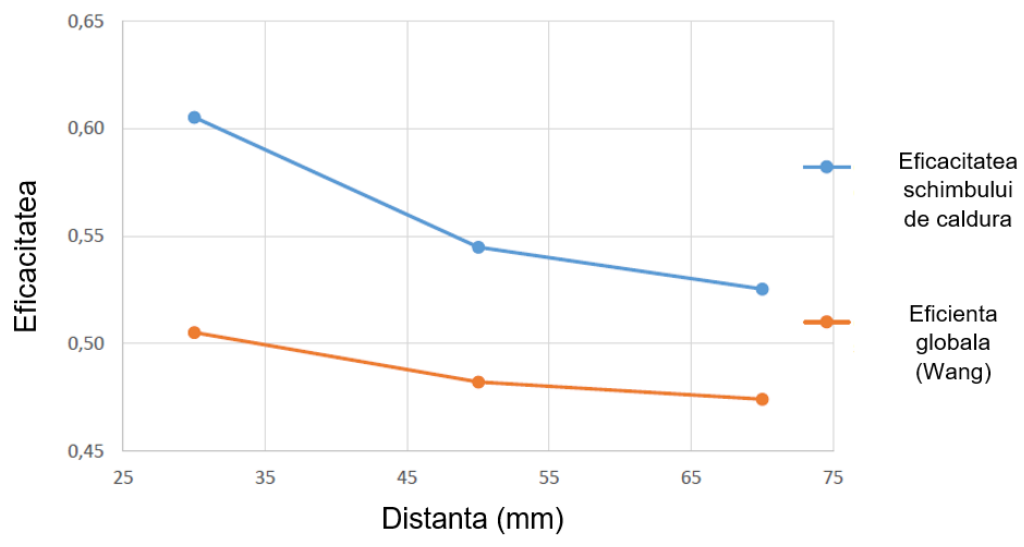


Figure 22 Efficiency and effectiveness of the solar collector

As in the preliminary study and in this case we can conclude that with increasing distances between the glass and the absorbent plate, the air temperature at the outlet decreases, thus increasing the average temperature of the absorbent plate, yields and efficiency for shorter distances being higher.

In the next chapter we will study closely both in terms of quantity and quality the two configurations for 30 mm and 50 mm.

## 4.5.4 Influence of the absorption coefficient of the perforated plate and the transmission coefficient of the glass

A recent study was conducted to find out how the absorption coefficient of the perforated plate and the transmission coefficient of the glass can influence the efficiency of the solar collector. These two parameters are constant related to the properties of the materials and their color. The absorption coefficient represents the property of a material to absorb solar radiation, maximum value being 1, it belongs to the "black body", and the second parameter represents the property of glass to

transmit solar radiation and thus received energy. In the following were described the parameters that changed and the parameters that remained at the same value for the simulations performed.

Table 9 Parameters used in numerical simulations - influence of the absorption coefficient of the perforated plate and the transmission coefficient of the glass

|                        | Parametrii                    | Valori             |
|------------------------|-------------------------------|--------------------|
| Boundary<br>conditions | Inlet temperature (°C)        | 25                 |
|                        | Air flow (m <sup>3</sup> /h)  | 158                |
|                        | Distance (mm)                 | 30                 |
|                        | Date                          | 11 oct. 13:00      |
|                        | Solar radiation               | Solar rad. 785 W   |
|                        | Absorption coefficient of the | 0,6; 0,8; 0,9      |
| Variable               | perforated plate              |                    |
|                        | The transmission coefficient  | 0,4; 0,7; 0,8; 0,9 |
|                        | of the glass                  |                    |

Below were graphically represented the influence of these parameters on the plate temperature and the outlet temperature of the glazed solar collector.

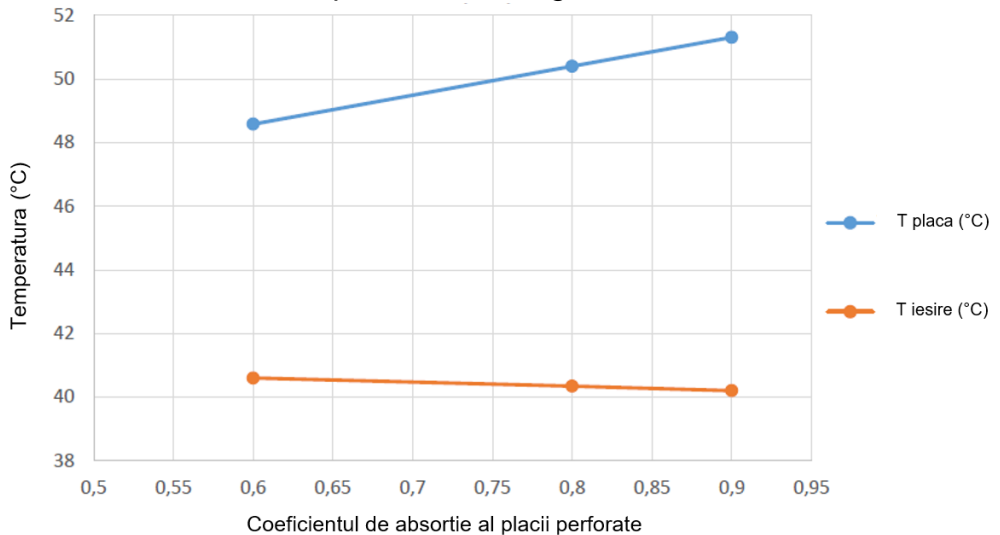


Figure 23 Influence of the absorption coefficient of the perforated plate on the plate temperature and the outlet temperature

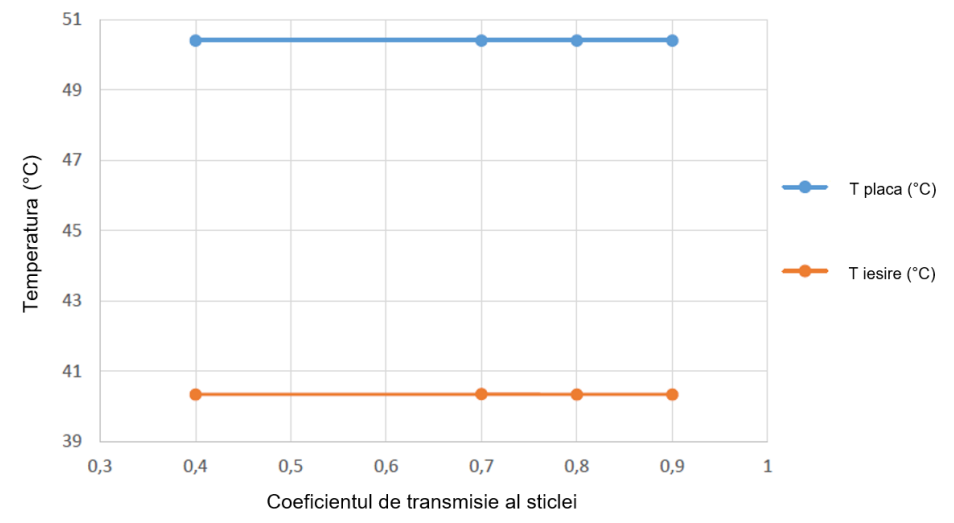


Figure 24 The influence of the transmission coefficient of the glass on the plate temperature and the outlet temperature

As the absorption coefficient of the plate increases and the plate temperature increases as seen in the graph above, however the outlet temperature decreases, an explanation for this phenomenon is that with the increase of the absorption coefficient, the transmission and reflection coefficient of the plate decreases in contact with the air, this being explained by the equation:

$$\alpha + \rho + \tau = 1$$
 (16)

,where:

 $\alpha$  -> the absorption coefficient of the material

ρ -> the reflection coefficient of the material

au -> the transmission coefficient of the material

As for the transmission coefficient of the glass, given the results obtained in the graph above, it does not influence the temperature values, this coefficient represents the fraction of light entering through the glass of the solar collector, these results may be erroneous due to the program that does not capture all the physical phenomena that occur in the glass.

#### 4.5.5 The influence of turbulence patterns

Knowing some of the most used turbulence models, it is proposed to compare the previously obtained values with a model that does not require a high computing power, more precisely the k- $\omega$  SST model, which better captures the phenomena near the plate compared to the standard k- $\omega$  .

The previous simulations were performed taking into account the boundary conditions within the experimental stand for the 6 cases of air flows through the collector for the inlet temperature, the flow and the solar radiation. Comparative graphs for  $\mathbf{k}$ - $\mathbf{\epsilon}$  realizable with  $\mathbf{k}$ - $\mathbf{\omega}$  SST are illustrated below.

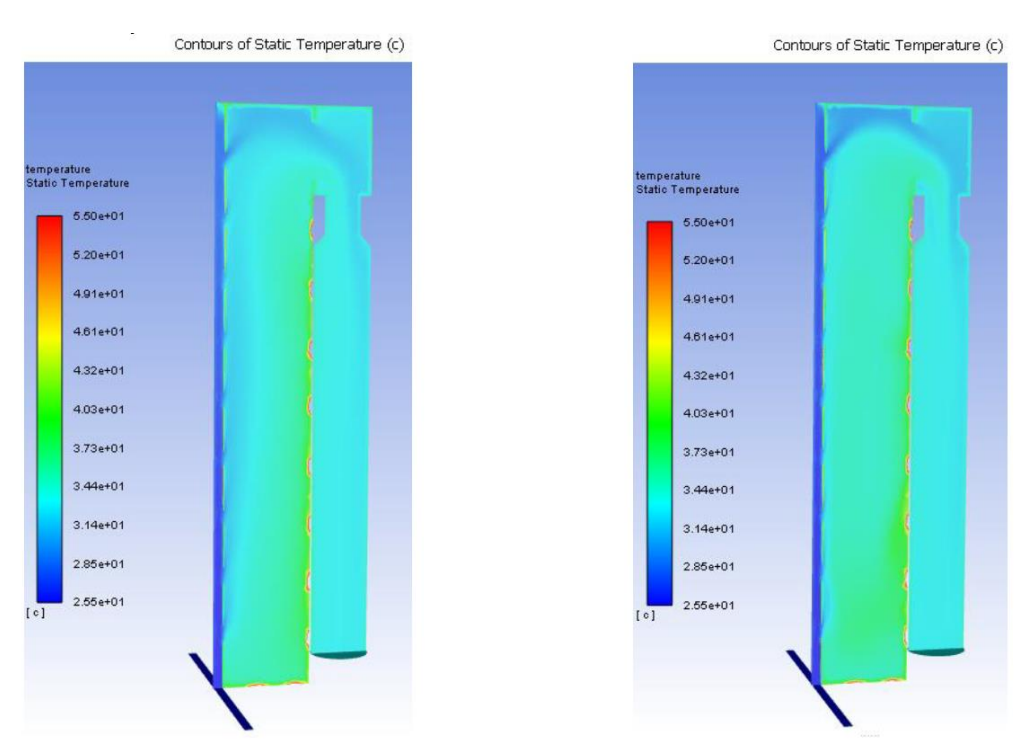


Figure 25 Turbulence models - temperature profile in the solar collector

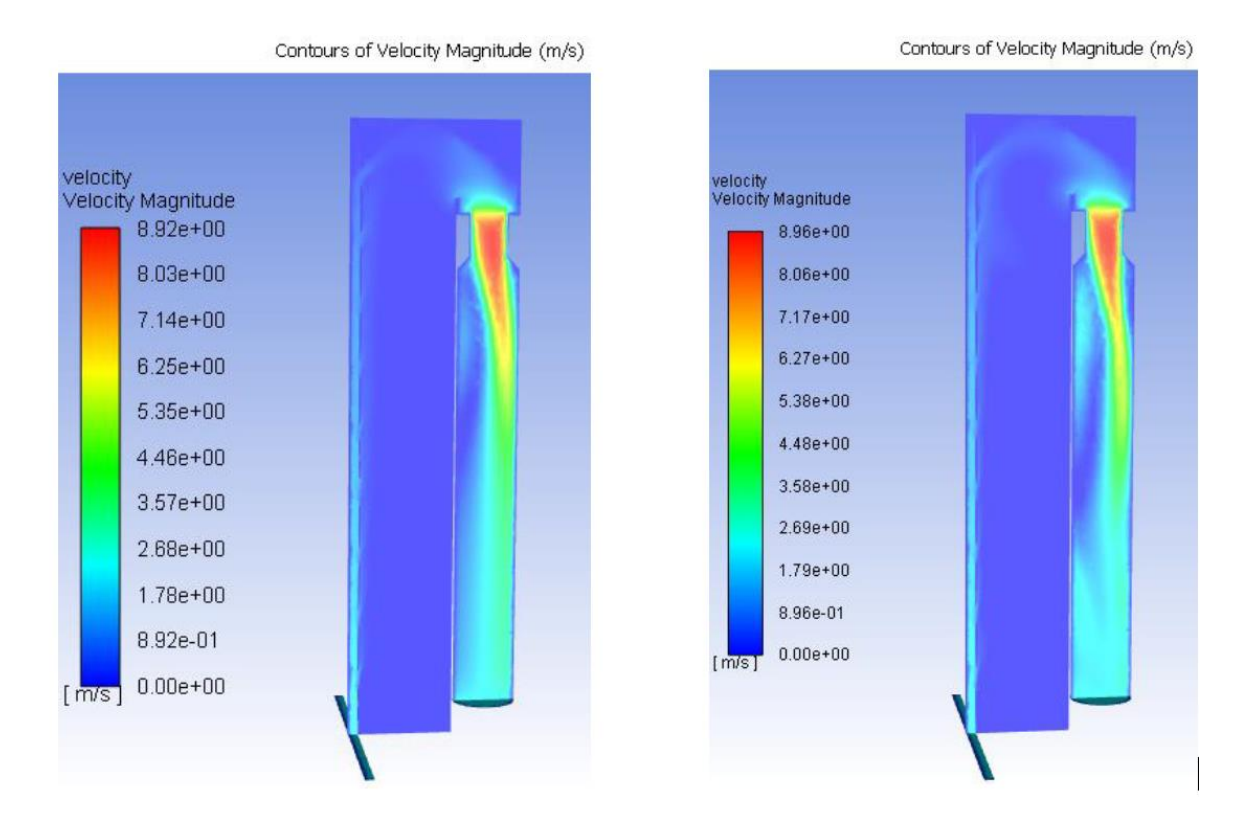


Figure 26 Turbulence models - velocity profile in the solar collector

It can be seen in the images above that the two turbulence models get almost identical results, a small difference can be seen in the velocity profile at the outlet of the manifold, so for the k- $\epsilon$  model the air flow is more stabilized at the outlet. Subsequently, the outlet temperature, the average plate temperature as well as the global efficiency and the efficiency of heat exchange are plotted graphically.

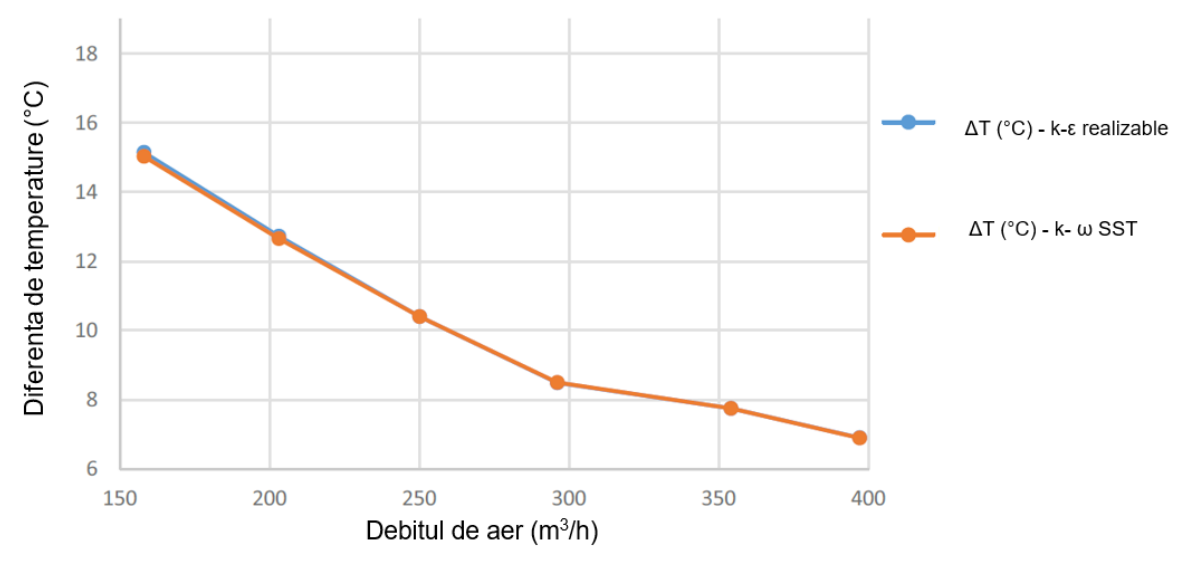


Figure 27 The temperature difference between the inlet and the outlet of the solar collector depending on the turbulence model

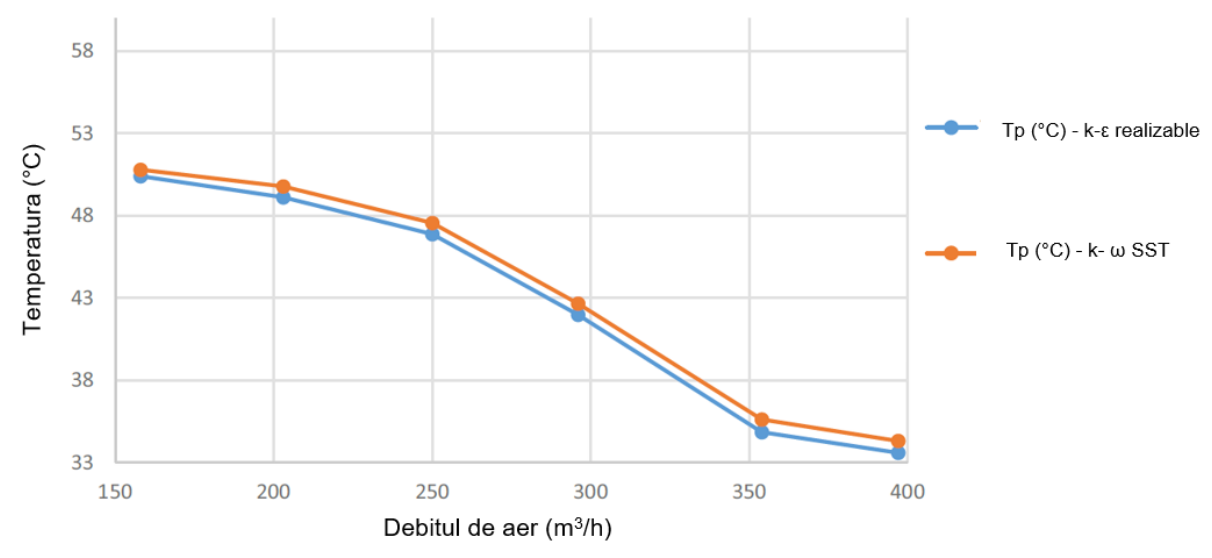


Figure 28 Average temperature of the perforated plate depending on the turbulence model

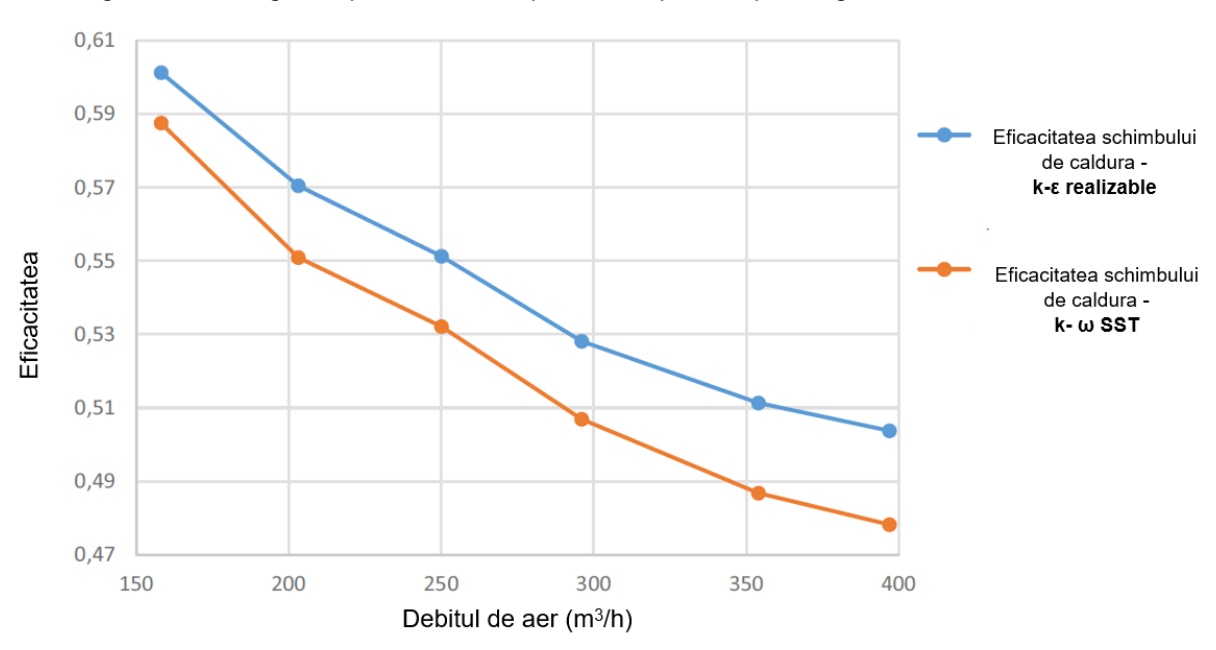


Figure 29 The efficiency of the solar collector depending on the turbulence model

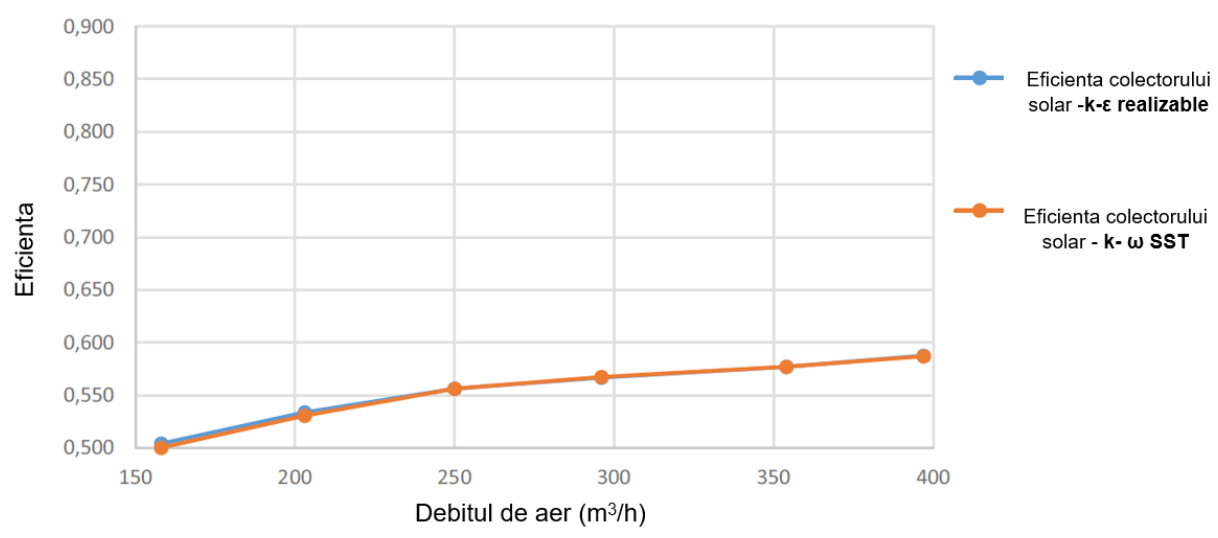


Figure 30 Solar collector efficiency depending on the turbulence model

As can be seen from the graphs above, the parameters studied do not show major differences for the turbulence model k- $\omega$  SST, thus obtaining a difference of 2% or about 0.7 ° C for the temperature of the perforated plate. This difference is reflected in a difference of 5% for the efficiency of heat exchange and a difference of 0.8% for the overall efficiency of the glazed solar collector.

Therefore a conclusion can be drawn for the glazed solar collector the turbulence model  $k-\omega$  SST is not more accurate than the achievable turbulence model  $k-\varepsilon$ , it can be explained by a reduced turbulence of the flow at the perforated plate.

These simulations were carried out in partnership with the I.N.S.A. of Lyon within the Research and Development Initiation Report (Rapport Projet Initiation à la Recherche et Développement - PIRD) together with the help of colleague Quentin TOURNOIS.

# 5. Comparative numerical study to determine the optimal configuration of the glazed solar collector

To perform the comparative numerical study, the Ansys Fluent 19.2 simulation software was used, in which the geometry was represented as figure 31 below, this geometry represents the geometric configuration of the experimental model of glazed solar collector with perforated plate. Thus the geometry is represented by a 2m x 1m glass panel mounted at a distance of 30 mm or 50 mm from the absorbent plate. The absorbent plate is made of aluminum with a thickness of 2mm and in which 181 perforations with dimensions of 50mm x 50mm were made, these being arranged as in figure 31.

In the following, a comparative study was performed between two solar collector solutions, having the same geometry, the difference between the two studies being the distance between the absorbent plate and the glass.

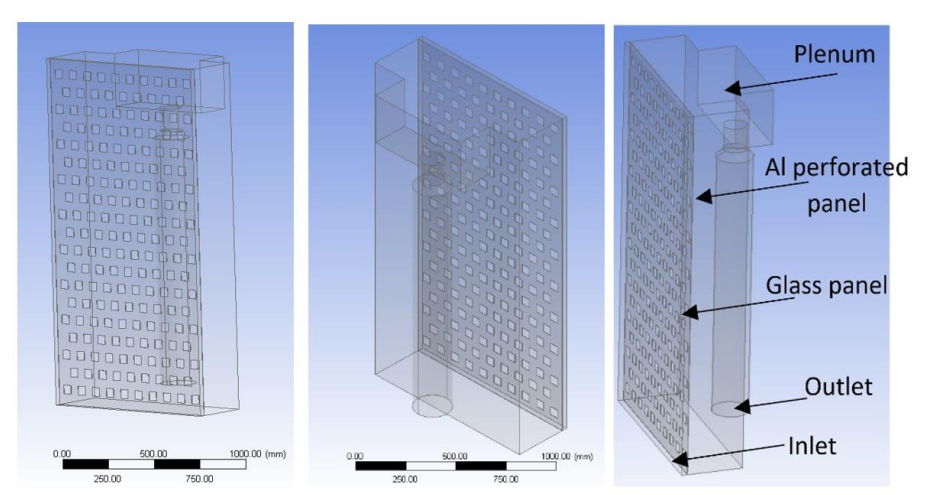


Figure 31 Geometry of the studied solar collector

In order to obtain better results with a consumption of resources and as little time as possible, an independence study was carried out for meshes with 714,000, 1,450,000, 2,950,000 and 4,130,000 tetrahedral elements. The mesh with 2.95 million tetrahedral elements was used for further studies, this is also due to the fact that the coarsely chosen perforations allowed the choice of larger distractions on the entire solar collector system.

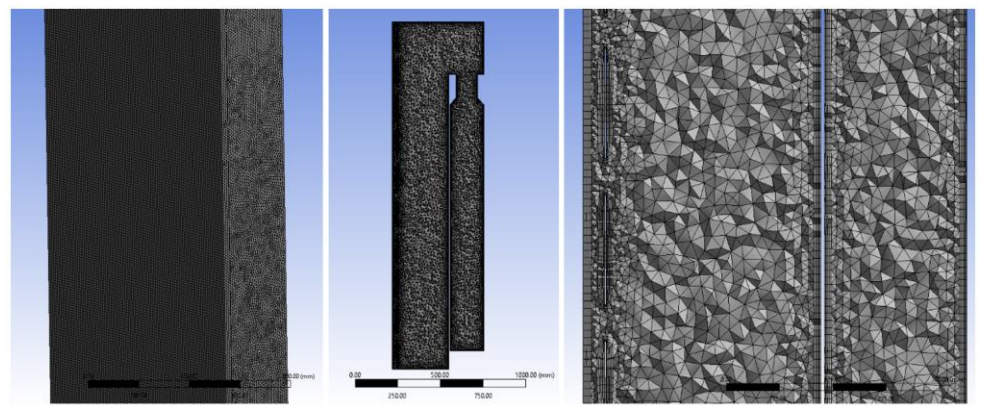


Figure 32 Making the mesh 2,950,000 tetrahedral elements

The turbulence model chosen for the comparative study is k- ε Realizable with Enhanced Wall Treatment for the section of Fluent Near-Wall Treatment [15], the energy equation was activated and the air was considered as the ideal gas.

The radiation and the position of the solar collector was calculated using the program inside Fluent, Solar Ray Tracing, thus having a direct radiation of 800 W/m² and diffuse radiation of 150 W/m², as the position of the solar collector was chosen the city of Timisioara, as a model The S2S (Surface-to-Surface) function has been activated.

For the entry into the solar collector as a boundary condition a pressure of 0 Pa was imposed, taking into account that the air is set in motion by means of a fan [14], as simulation flows the following flows were considered: 158, 203, 250, 296, 354, 397  $\,$  m<sup>3</sup> / h, conditions that were simulated and in the study of the parameters.

#### 5.1 Simulation results

The main objective of the study was to evaluate the temperature and velocity to determine the optimal configuration of the solar collector both in terms of air flow and the distance between the absorbent plate and the glass. Thus the simulation results for the two configurations were illustrated in the table below:

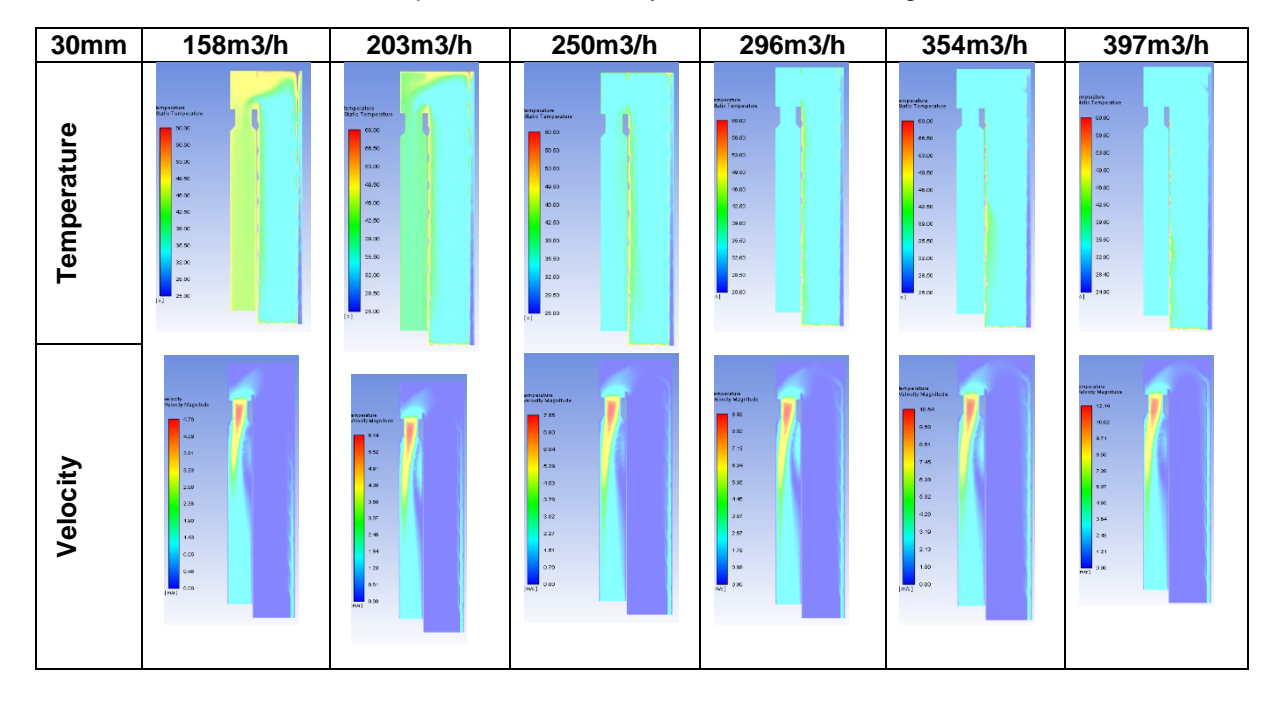


Table 10 Temperature and velocity field for 30mm configuration

According to the simulations illustrated above we can observe an increase in the outlet temperature for the case when the distance between the glass and the absorbent plate is 30 mm. The velocity field shows us that for lower air flows the air flow is only in the lower part of the solar collector and for higher flows the flow is uniform on the surface which means that more heat is extracted for the case of air flows.

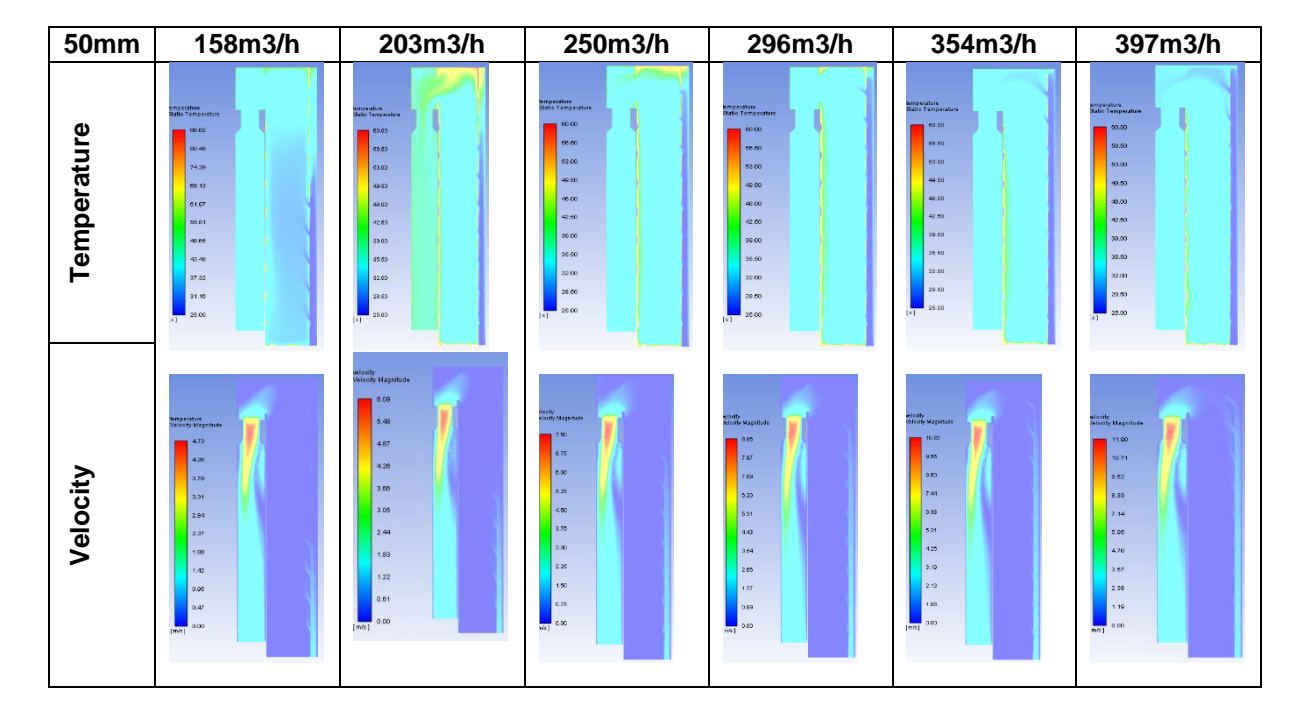


Table 11 Temperature and velocity field for 50mm configuration

As can be seen from the simulations performed for the 30 mm configuration, the highest temperature is for the lowest flow, more precisely 157 m $^3$  / h and for the 50 mm configuration the flow of 203 m $^3$ / h represents the situation when the outlet temperature is the highest, the increase in temperature compared to the inlet is in the range of 34% to 78%.

Calculating the efficiency of the solar collector it can be seen that for higher flow values and shorter distances the efficiency is higher.

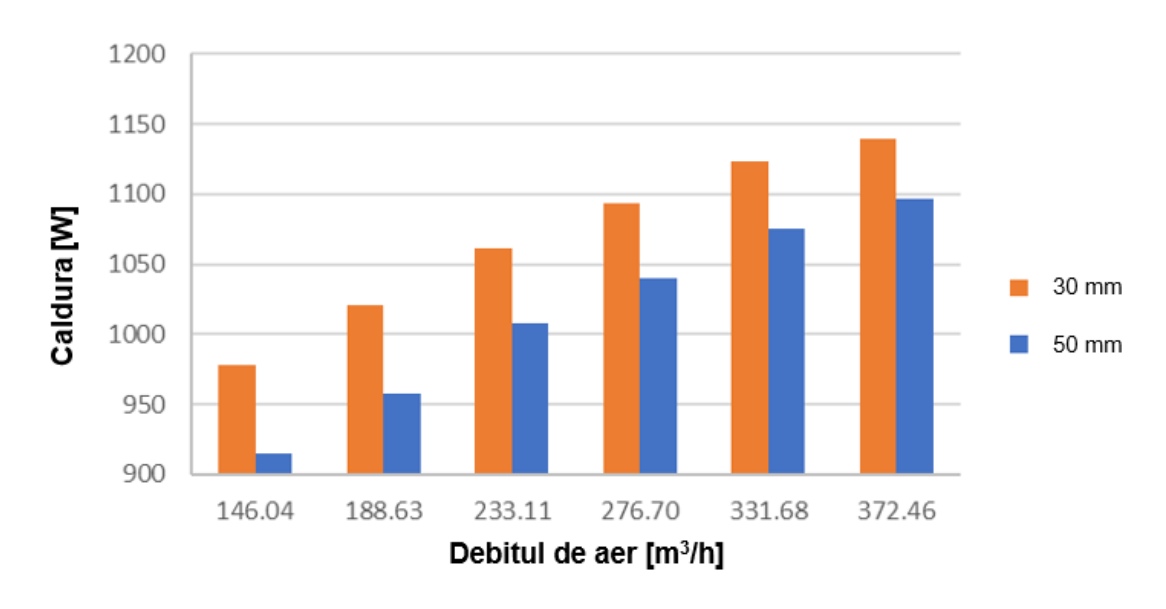


Figure 33 Heat extracted according to flow - distance study

If the efficiency of the solar collector is calculated, its values vary between 50% to 61% for the distance of 30 mm and for the distance of 50 mm between the absorbent

plate and the glass, the efficiency of the collector is between 41% and 54% indicates that a shorter distance brings an area where the air heats up faster.

In order to calculate the overall efficiency of the two collectors, a study of the pressure loss was performed, it can be seen that the difference between the two configurations is small, indicating that for the distance of 30 mm it is more efficient than the 50 mm, having the same consumption. fan power

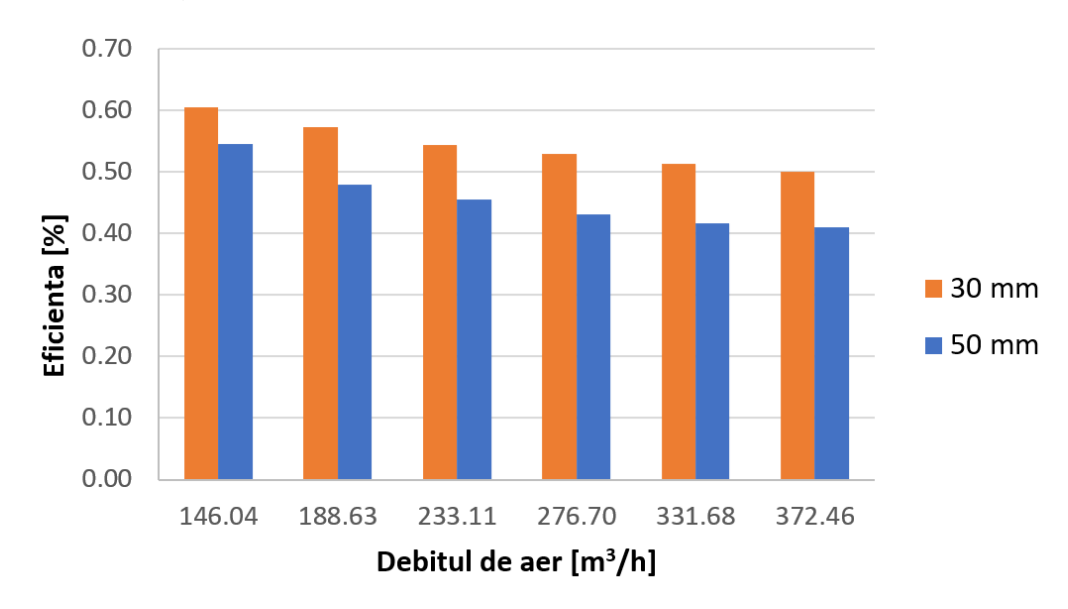


Figure 34 Efficiency of the solar collector depending on the flow - distance study

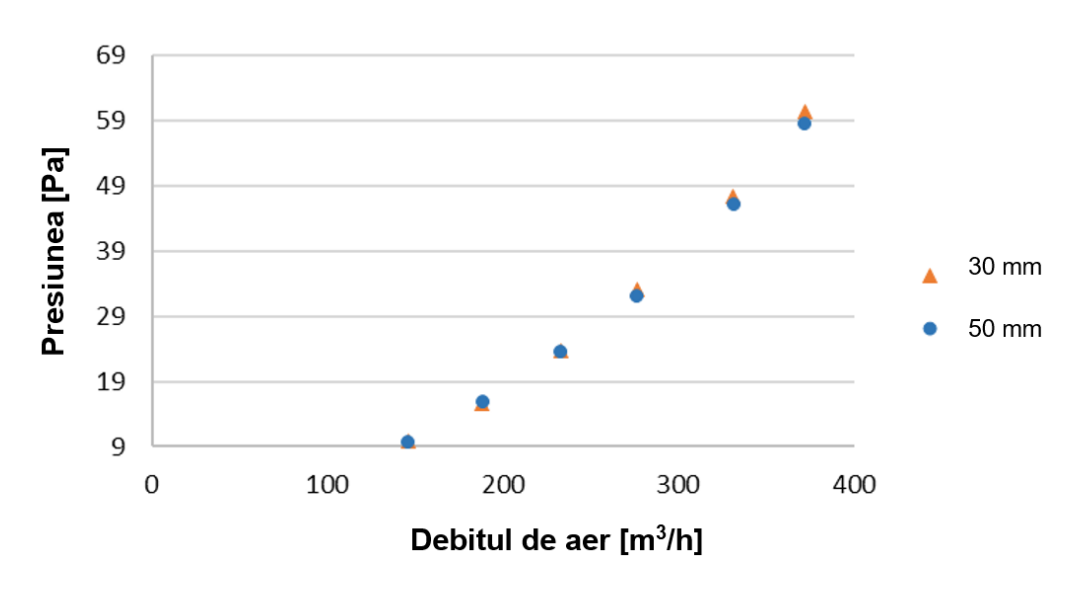


Figure 35 Pressure loss depending on air flow - distance study

In conclusion, the configuration with a smaller distance between the absorbent plate and the glazed surface is more efficient for all considered flows, so for a flow of  $158 \ m^3$  / h, the extracted heat was  $980 \ W$  and for the  $50 \ mm$  configuration the heat was  $60 \ W$  more little which indicates that the distance of  $30 \ mm$  between the absorbent plate and the glazed surface is the optimal option in terms of the solar collector.

#### 6. Conclusions

The building sector is responsible for a third of total energy consumption and CO<sub>2</sub> emissions being the most important sector where energy consumption can be reduced with a minimum of effort. To achieve these goals it is necessary to implement efficient passive systems and solutions that use renewable energy sources so as to obtain comfort parameters with a minimum of energy. [31] [32]

One such system that uses renewable energy sources is glazed solar collectors with perforated absorbent plate, a system that has been considered to determine the optimal configuration that will be implemented in future studies of smart facades or active facades.

The results obtained in numerical studies show the potential of this type of solar collector for preheating the air in boiler ventilation systems. By adding the glazed surface, the influence of the wind on the solar collectors is reduced, thus increasing the overall efficiency of this type of collector. The structure presented above can be used, thus having promising results for heating as well as ventilation of the interior spaces, as it is shown in the studies in the literature. The validated CFD model can thus be further used for new configuration improvements, the solution that offers the best results being the 30 mm solution. [19] [33] [11]

### 7. Conferences and publications

- Cătălin Sima, Cătălin Teodosiu, Cristiana Croitoru, Florin Bode Experimental study of heat transfer inside a real scale innovative air solar collector, EENVIRO 2020, 21 - 23 October, Bucharest, Online Conference
- 2. Cătălin Teodosiu, Cătălin Sima, Cristiana Croitoru, Florin Bode Analysis of velocity and temperature fields inside an air solar collector A numerical approach EENVIRO 2020, 21 23 October, Bucharest, Online Conference
- 3. Catalin Sima, Catalin Teodosiu, Charles Berville Mesh independency study for a solar glazed transpired collector, Building Services and Energy Efficiency July 2, 2020 July 3, 2020 Iaşi, Romania
- 4. Catalin Sima, Catalin Teodosiu, Abraham Tetang Fokone, Andrei -Stelian Bejan -Elements of influence for solar ventilated building facades: a review, DSC 2019: 2nd Conference of the UTCB Doctoral School, Technical University of Civil Engineering Bucharest, October 25, 2019
- Anca Bodale, Tiberiu Catalina, and Sima Cătălin-Ionuț Adaptation of buildings to climate change through bioclimatic strategies, in Romania, CLIMA 2019 Congress web of Conferences 26-29 May 2019, E3S Web of Conference 111, 06071(2019), DOI:10.1051/e3sconf/201911106071

#### 8. References:

- [1] ExxonMobil, "2017 The Outlook for Energy: A View to 2040 Contents," 2017. DOI:10.1080/01998595.2012.10491656.
- [2] a U.S. Energy Information, "Annual Energy Outlook 2015 with projections to 2040," 2015. DOI:DOE/EIA-0383(2013).
- [3] NASA, "NASA National Aeronautics and Space Administration (SUA). NOAA Data Show 2016 Warmest Year on Record Globally. Washington DC, SUA," website 25.08.2019, 2018. https://www.nasa.gov/press-release/nasa-noaa-data-show-2016-warmest-year-on-record-globally (accessed Aug. 25, 2019).
- [4] C. M.B., "Contribuţii la dezvoltarea modelului matematic gray box utilizat în analiza clădirilor cu înaltă eficienţă energetică," Universitatea Politehnica Bucureşti, România, 2015.
- [5] E. Mlecnik, *Innovation development for highly energy-efficient housing:*Opportunities and challenges related to the adoption of passive houses. 2013.
- [6] C. Reichl, K. Kramer, C. Thoma, P. Benovsky, and T. Lemée, "Comparison of modelled heat transfer and fluid dynamics of a flat plate solar air heating collector towards experimental data," *Sol. Energy*, vol. 120, pp. 450–463, Oct. 2015, DOI:10.1016/j.solener.2015.07.011.
- [7] C.-M. Lai and S. Hokoi, "Solar façades: A review," *Build. Environ.*, vol. 91, pp. 152–165, Sep. 2015, DOI:10.1016/j.buildenv.2015.01.007.
- [8] K. Hami, B. Draoui, and O. Hami, "The thermal performances of a solar wall," *Energy*, vol. 39, no. 1, pp. 11–16, Mar. 2012, DOI:10.1016/j.energy.2011.10.017.
- [9] R. K. Goyal, G. N. Tiwari, and H. P. Garg, "Effect of thermal storage on the performance of an air collector: A periodic analysis," *Energy Convers. Manag.*, vol. 39, no. 3–4, pp. 193–202, Feb. 1998, DOI:10.1016/S0196-8904(96)00226-9.
- [10] M. A. Leon and S. Kumar, "Mathematical modeling and thermal performance analysis of unglazed transpired solar collectors," *Sol. Energy*, vol. 81, no. 1, pp. 62–75, Jan. 2007, DOI:10.1016/i.solener.2006.06.017.
- [11] L. Gao, H. Bai, and S. Mao, "Potential application of glazed transpired collectors to space heating in cold climates," *Energy Convers. Manag.*, vol. 77, pp. 690–699, Jan. 2014, DOI:10.1016/j.enconman.2013.10.030.
- [12] M. M. Alkilani, K. Sopian, M. A. Alghoul, M. Sohif, and M. H. Ruslan, "Review of solar air collectors with thermal storage units," *Renew. Sustain. Energy Rev.*, vol. 15, no. 3, pp. 1476–1490, Apr. 2011, DOI:10.1016/j.rser.2010.10.019.
- [13] A. Shukla, D. N. Nkwetta, Y. J. Cho, V. Stevenson, and P. Jones, "A state of art review on the performance of transpired solar collector," *Renewable and Sustainable Energy Reviews*. 2012, DOI:10.1016/j.rser.2012.02.029.
- [14] D. N. Nkwetta and F. Haghighat, "Thermal energy storage with phase change material—A state-of-the art review," *Sustain. Cities Soc.*, vol. 10, pp. 87–100, Feb. 2014, DOI:10.1016/j.scs.2013.05.007.
- [15] T. Zhang, Y. Tan, H. Yang, and X. Zhang, "The application of air layers in building envelopes: A review," *Appl. Energy*, vol. 165, pp. 707–734, Mar. 2016, DOI:10.1016/j.apenergy.2015.12.108.
- [16] K. Januševičius, G. Streckiene, J. Bielskus, and V. Martinaitis, "Validation of Unglazed Transpired Solar Collector Assisted Air Source Heat Pump Simulation Model," 2016, DOI:10.1016/j.egypro.2016.09.039.
- [17] C. Brown, E. Perisoglou, R. Hall, and V. Stevenson, "Transpired Solar

- Collector Installations in Wales and England," *Energy Procedia*, vol. 48, pp. 18–27, 2014, DOI:10.1016/j.egypro.2014.02.004.
- [18] X. Wang, B. Lei, H. Bi, and T. Yu, "A simplified method for evaluating thermal performance of unglazed transpired solar collectors under steady state," *Appl. Therm. Eng.*, vol. 117, pp. 185–192, May 2017, DOI:10.1016/j.applthermaleng.2017.01.053.
- [19] W. Zheng, B. Li, H. Zhang, S. You, Y. Li, and T. Ye, "Thermal characteristics of a glazed transpired solar collector with perforating corrugated plate in cold regions," *Energy*, vol. 109, pp. 781–790, Aug. 2016, DOI:10.1016/j.energy.2016.05.064.
- [20] B. Nábìlek, E. Kiran, F. Türksoy, and A. Yazar, "Performance of an unglazed textile-plastic solar absorber," *Renew. Energy*, vol. 16, no. 1–4, pp. 635–638, Jan. 1999, DOI:10.1016/S0960-1481(98)00241-9.
- [21] P. K. Bansal and S. C. Kaushik, "Diurnal response of solar air heaters," Appl. Energy, vol. 9, no. 2, pp. 107–120, Oct. 1981, DOI:10.1016/0306-2619(81)90047-7.
- [22] H. K. Versteeg, W. Malalasekera, G. Orsi, J. H. Ferziger, A. W. Date, and J. D. Anderson, *An Introduction to Computational Fluid Dynamics The Finite Volume Method.* 1995.
- [23] J. F. Wendt et al., Computational fluid dynamics: An introduction. 2009.
- [24] C. Teodosiu, *Modelarea si simularea sistemelor in domeniul instalatiilor pentru constructii.* Matrix Rom, 2007.
- [25] V. D. Liseikin, *Grid Generation Methods*. 2009.
- [26] "ANSYS FLUENT 12.0 Theory Guide 4.5.1 Standard Model." https://www.afs.enea.it/project/neptunius/docs/fluent/html/th/node66.htm (accessed Sep. 13, 2021).
- [27] "Which Turbulence Model Should I Choose for My CFD Application? | COMSOL Blog." https://www.comsol.com/blogs/which-turbulence-model-should-choose-cfd-application (accessed Sep. 13, 2021).
- [28] P. Charvát, L. Klimeš, O. Pech, and J. Hejčík, "Solar air collector with the solar absorber plate containing a PCM Environmental chamber experiments and computer simulations," *Renew. Energy*, 2019, DOI:10.1016/j.renene.2019.05.049.
- [29] T. Zhang, Y. Tan, X. Zhang, and Z. Li, "A glazed transpired solar wall system for improving indoor environment of rural buildings in northeast China," *Build. Environ.*, vol. 98, pp. 158–179, Mar. 2016, DOI:10.1016/j.buildenv.2016.01.011.
- [30] G. W. E. Van Decker, K. G. T. Hollands, and A. P. Brunger, "Heat-exchange relations for unglazed transpired solar collectors with circular holes on a square or triangular pitch," *Sol. Energy*, vol. 71, no. 1, pp. 33–45, 2001, DOI:10.1016/S0038-092X(01)00014-7.
- [31] European Commission, "Communication from the Commission to the European Parliament and the Council: The Paris Protocol A blueprint for tackling global climate change beyond 2020," *J. Chem. Inf. Model.*, 2015.
- [32] Transition to sustainable buildings: Strategies and opportunities to 2050. 2013.
- [33] X. Li, C. Li, and B. Li, "Net heat gain assessment on a glazed transpired solar air collector with slit-like perforations," *Appl. Therm. Eng.*, 2016, DOI:10.1016/j.applthermaleng.2015.12.069.